Damage of Functionalized Self-Assembly Monomolecular Layers Applied to Silicon Microgear MEMS

Nabeel Almuramady[1, 2], Feodor M. Borodich[1], Irina G. Goryacheva[3] and Elena V. Torskaya[3]

[1]School of Engineering, Cardiff University, Cardiff, Wales, UK, CF24 3AA
[2]College of Engineering, University of Al-Qadisiyah, Al-Qadisiyah, Iraq
[3]Tribology Lab., Ishlinsky Institute for Problems in Mechanics, Russian Academy of Sciences, Moscow, Russia

Abstract

Tooth surfaces of silicon-based MEMS microgears are described as smooth surfaces covered by adhesive asperities (nanoblocks). To reduce adhesive effects, the tooth surfaces are functionalized by OTS-SAM (Octadecyltrichlorosilane self-assembly monomolecular) carbon-based functionalized coatings. The wear of the coating is modelled using the modified Goryacheva-Torskaya model of damage accumulation. The amount of energy dissipated by different physical and chemical mechanisms along with energy dissipated by mechanical deformation of the counterparts is used to evaluate the frictional force. The main scenarios of wear process within the coating are described and discussed. The damage evolution is described for several levels of external load

Keywords: fatigue wear; adhesion; friction; sliding.

1. Introduction

Micro-Electro-Mechanical Systems (MEMS) can be of various kinds depending on the specific industrial or space applications [1-4]. MEMS consist of a significant number of micro/nano components and the majority of them work in contact with each other to transfer the load and torque between MEMS parts. Adhesion is the key issue for the MEMS devices that highly restricts the movements of the micro/nano elements [5, 6]. Here we defined stiction as the unintentional adhesive connection between the teeth that does not allow MEMS to work at all. Stiction may lead to structure failure or significantly reduces the MEMS reliability [7, 8]. Adhesive interactions between surfaces may be greatly affected by environmental conditions. Here we focus on clean MEMS surfaces working in the vacuum environment when one of the leading mechanisms of stiction is cold welding (cohesion) between micromachined surfaces, while the capillary adhesion and effects of gaseous environment are out the scope of this study. If the teeth of a microgear MEMS are simulated as working in the vacuum environment then, the mechanisms of the energy dissipation may be reduced to the following: (i) dissociation of chemical and van der Waals bonds, and (ii) the elastic interlocking between counterpart's proturberances. One of the successful solutions that allows the researchers to reduce cohesion and, therefore, to eliminate stiction is surface functionalization [1]. Carbon-based functionalized coatings have commonly been used in friction and sliding conjunctions to improve the lifetime expectations of the surfaces. Many researchers have tried to investigate and model this problem to reduce the effect of friction and wear on the contacting surfaces [8, 9]. Tribology of self-assembled monolayers has been intensively studied in many papers (see, e.g. [10-15]). Indeed, the adsorbed organic molecules that are organized into oriented layers may drastically change the surface properties of contacting solids. It was observed experimentally that friction of surfaces covered by molecular self-assembled monolayers has anisotropic properties [10]. It was also shown that thin diamond-like carbon films covered by octadecyltrichlorosilane self-assembled monolayers exhibit considerable reduction of friction due to its ultra-low surface energy and special film structure [14]. If such a layer is used to cover titanium films then they exhibit hydrophobic and improved tribological properties [15]. The properties of monomolecular layers can be studied both theoretically [16-18] and experimentally [10-13]. It was shown that for a single-crystal strip, the Young modulus increases with decreasing thickness of the strip; in particular, the elastic modulus of a very thin crystal film consisting of two atomic layers can differ from its macroscopic value by a factor of two [17]. It is clear that the functionalized coatings may be worn away; therefore, studies of wear of the functionalized layers are of great importance for modern nano/micro technology.

Self-assembled monomolecular (SAM) layers are often used to functionalize the silicon surfaces of the microdevices. Generally, the SAM layers are formed by exposing silicon substrate to the vapour phase of the desired molecule and incubation for some time. Here we will study OTS-SAM (Octadecyltrichlorosilane SAM)

layers that are often used to functionalize silicon surfaces. These types of SAM functionalized layers are consisting of head, terminal and spacer groups (see Figure 1).

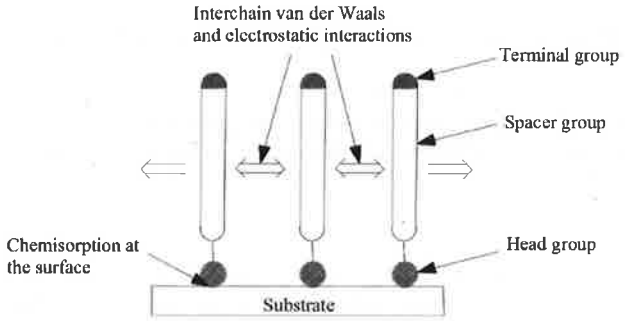

Figure 1. Self-assembled monomolecular layer on a silicon substrate and the corresponding intermolecular forces (adapted from [9])

The molecular spacer group or simply a spacer is any flexible part of a molecule that is providing a good linking between two other parts of a molecule. The head is chemisorbed to the substrate and the molecular adsorption brings the SAM molecules close enough to each other and, therefore, the short-range van der Waals forces and electrostatic interactions become important [9]. As it will be shown below, the use of the OTS-SAM layer will reduce considerably the amount of the dissipated energy and, in turn, the friction force. Therefore, the temperature will be practically the same and the temperature effects may be neglected until the functionalized monomolecular layer has been not worn away.

Here a damage model is presented that describes the damage accumulation related to dissociation of chemical bonds, electrostatic and van der Waals interactions among the elements of the SAM head and spacer groups. The damage leads eventually to wear of these carbon-based functionalised monomolecular layers. The model is based on the Goryacheva-Torskaya model [19, 20] for damage accumulation in fatigue elements. The maximum damage occurs under action of the maximum load, hence the dry friction contact of a single tooth contact is considered.

To use the damage model, the surface stresses are calculated. The MEMS tooth roughness is described using statistical approach in accordance with the experimental data obtained by Atomic Force Microscopy (AFM). In the simulations, the rough MEMS teeth are described as smooth curved tooth surfaces covered by adhesive nanoblocks representing the asperities. Each nanoblock is obtained by superposition of two hierarchical subscales that are specified by the character of interactions at the subscale: an atomic subscale, where chemical interactions are likely to occur, and adhesive subscale, where molecular adhesion (van der Waals interaction) is significant. Numerical simulations for silicon-based MEMS micro-tooth surfaces functionalised by monomolecular carbon-based coatings show that initially the surfaces do not stick to each other. However, the stiction occur after some number of cycles because the functionalised monomolecular is gradually worn away due to damage accumulation in the layer [21, 22]. It is shown that the coatings wear occurs not simultaneously, because the atomic subscale element located at the corner of the nanoblock will have higher stresses than other atomic subscale elements of the nanoblock. The damage evolution is discussed and described for several levels of external load.

2. The MEMS surface topography and models of dry friction

2.1 The MEMS surface topography.

The real silicon rough surface of a MEMS tooth may be described at different scales: nanoscale and bulk elastic scale. The nanoscale may be subdivided to the atomic and molecular subscales. The former is defined as the region of active chemical interactions, while the latter may be defined as the region of active van der Waals interactions, This is in accordance with a one-level model (the B-S model) presented recently the Borodich and Savencu [23] (for further details see also [24, 25]). Their model may be used to describe tribological

phenomena of nominally flat dry surfaces. Here the B-S model has been developed to describe the specific features of interactions between MEMS teeth [21, 22]. Contrary to the B-S model it is assumed here that the contacting surfaces have microscale curvature and, therefore the gap of a gear MEMS pair is continuously changing during the mesh cycle. To take this feature into account, an iterative approach was used based on a combination of solutions to 2D frictional Hertz-type problems obtained by the Cardiff contact solver [21, 27, 28, 29].

The B-S model is based on multiscale approach where the term 'scale' is related to the capabilities of the system to reflect different physical-chemical mechanisms of interactions between surfaces [23-25]. They considered the following scales: (i) atomic scale reflects the phenomena specific to the characteristic length $l \leq 1\ nm$, namely chemical interactions between surfaces; (ii) nanoscale reflects phenomena specific to the characteristic length $1\ nm \leq l \leq 1\mu m$, mainly the van der Waals interaction between surfaces; (iii) microscale is attributed to phenomena specific to the characteristic length $1\mu m \leq l \leq 1mm$, namely the mechanical interlocking of asperities, and (iv) macroscale is attributed to phenomena specific to length scale over $1mm$, including the behaviour of the bulk of the body, which will couple the micro-asperities together.

The main structure of the multiscale frame has been characterised using statistics of the surface topography depending on the cross-section area at the specific subscale (see Figure 2). The model has been designed to consist of a hierarchical multiscale asperity structure and the supported rigid surface meshed, in addition to the sliding relative motion. Park XE-100 AFM device, which is well described by Brousseau et al. [30], has been used to test silicon surfaces. The hierarchical multiscale asperity block is characterised to reflect the physical and mechanical properties for the actual surface of the microgear MEMS tooth.

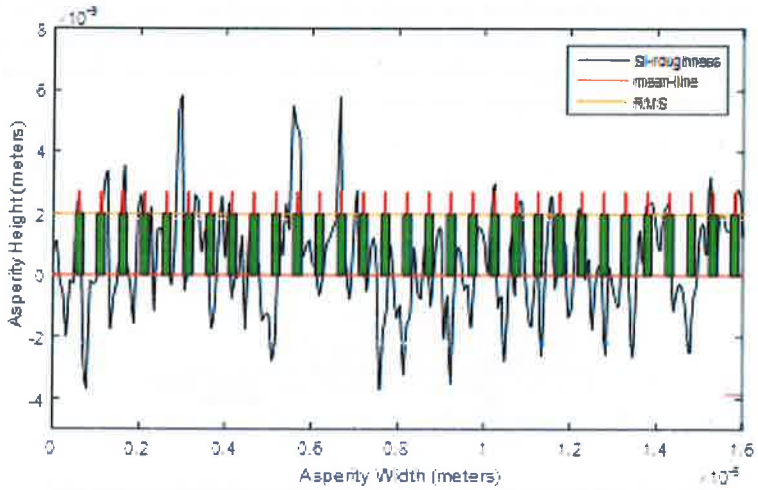

Figure 2. Computation of the width of the chemical and the van der Waals (green zones) interaction subscales for silicon roughness profile

The height and width of the adhesive subscale asperities were calculated by determining the area of the surface, which is limited between the mean line and the root mean square for the silicon roughness profile (Fig. 2). The nano-asperities were modelled as equally spaced rectangles on the tip of the micro-asperities. The height of the asperities was computed using root mean square of all asperity heights R_q, with respect to the mean-line of the profile

$$R_q = \sqrt{\frac{1}{n}\sum_{i=1}^{n} h_i^2} \tag{1}$$

where h_i are the heights of the discrete points of the measured nano-roughness, and n is the number of points.

Because the nano-asperity models both the chemical and the vdW interactions, it has two characteristic widths and two characteristic heights. If the nano-asperity is within the adhesive layer, then it has contact due to van der Waals forces. In this case w_{vdW} is the size of adhesive contact and w_{chem} is the size of chemical contact. The

width of the van der Waals interaction domain was computed by equally distributing the asperity volume bounded by the mean-line and the height of the van der Waals interaction slab, to the number of asperities in this window

$$w_{vdW} = \frac{A_{vdW}}{h_{rms}\, n_{mean}} \tag{2}$$

where A_{vdW} is the area hatched in Fig.2, h_{rms} is the quadratic mean of all asperity heights and n_{mean} is the number of asperities intersected by the mean-line.

At atomic subscale the silicon surface roughness was measured by an AFM (see for example [21,22]). As it has been described above, calculating the number of asperities at the representative length of the surface profile and applying statistical analysis, the height and width of the atomic subscale asperity, as well as the distance between the asperities were determined.

The distance between nano-asperities is computed as

$$\lambda = \frac{L_{nano}}{n_{mean}} \tag{3}$$

where L_{nano} is the length of the sampling profile [25]. The height of the chemical interaction slab was computed as the arithmetic average of all asperity heights above the height of the van de Waals interaction slab. The width of the chemical interaction domain is computed in a similar way to the width of the van der Waals interaction domain. The volume of the asperities above the height of the quadratic mean of asperity heights is equally distributed to all nano-asperities. The resulting approximation is illustrated in Figure 2. One should not be deceived by the aspect ratio in these figures as the scales of the axes are different. This value of the topography cross-section area is then equally redistributed, as shown in Figure 3.

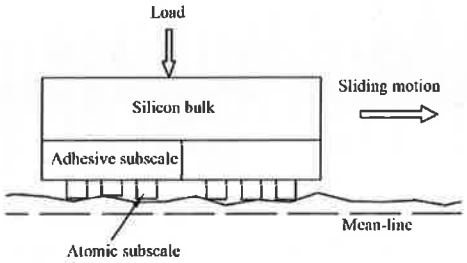

Figure 3. A multi-scale hierarchical structure with a vertical degree of freedom

In this geometry, the width of the adhesive subscale asperity has been calculated to be equal to $195\ nm$, the atomic subscale asperity width equal to $19.5\ nm$.

In the current model, micro-tooth surface has been modeled, as a bulk silicon MEMS surface covered by nano-sized roughness whose asperities are represented by nanoblocks having two subscales specified by the character of interactions: atomic subscale, where the chemical interactions are significant, and adhesive subscale, where the van der Waals interactions are likely occurred [22]. The adhesive subscale of a nanoblock have the same thickness, in fact it is an adhesive layer that is defined employing ideas of the Maugis step-function approximation [27]. The adhesion force of each nanoasperity has assumed to be equal to the pull-off force in the non-slipping Boussinesq-Kendall model solved by Borodich and using his no-slip coefficient [21, 22].

In this section, sliding microgear MEMS teeth (a silicon surface covered by nano-sized roughness) is functionalized by an OTS-SAM coating layer (see Figure 4a). The nanoasperities blocks are located over the micro-tooth surface and the nano-blocks are distributed at the nodes of a square lattice, as shown in Figure 4b and 4c. The microgear MEMS meshing teeth system was under the effects of nominal pressure, pt, and friction force.

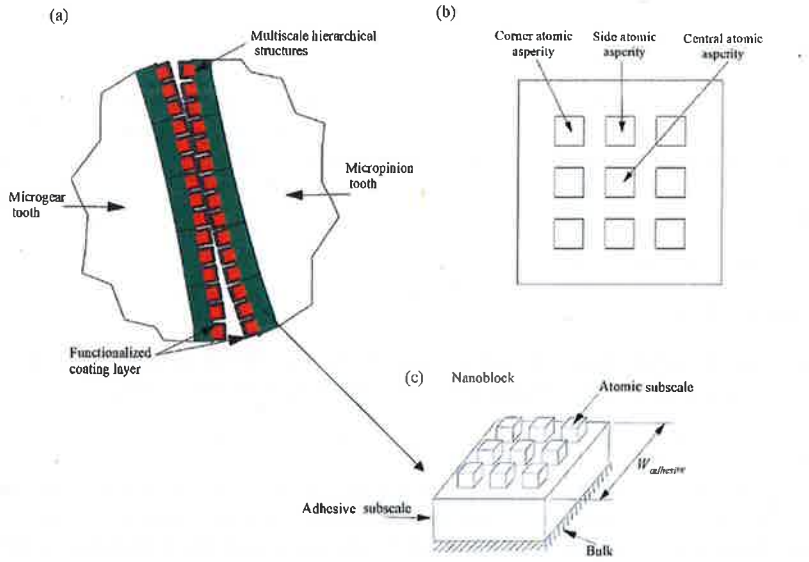

Figure 4. Hierarchically organised multiscale asperities over the surface of microgear tooth: a) a silicon microgear tooth (gray) is covered by adhesive layer (green)with superimposed atomic scale asperities (red), and the whole structure is covered by an OTS-SAM coating layer (black); b) a plane view of a nano-block covered by atomic scale asperities; c) a nanoblock representing a MEMS asperity.

2.2 Calculation of friction force.

The total friction force taken into account adhesion effect is determined depending on the total energy U_{diss} dissipated through the contact cycle

$$F_f = U_{diss}/x, \tag{4}$$

where F_f is the sliding friction force and x is the sliding distance over MEMS tooth. This energy lost is due to elastic deformation of nanoasperity over the sliding distance and dissociation of chemical and van der Waals bonds. Let us estimate the contributions of these components.

For a pure silicon surface, the dissociation of energy due to break the chemical bonds between two silicon atoms [31] is equal to *327 kJ/mol*, hence the energy of one chemical bond is *5.4e-19 J*. It is assumed that if silicon atoms of the atomic scale asperities contact the silicon atoms of the counterpart then all contacting atoms create chemical bonds; in addition, if the chemical bonds are broken due to sliding then the atoms create immediately new bonds with the counterpart atoms within the contacting (overlapping) regions of the atomic subscale. Then the total energy ($U_{Totalchem}$) dissipated by chemical bonds at the moment (t) is

$$U_{Totalchem}(t) = n_{atoms}(t)\, U_{chem} \tag{5}$$

where U_{chem} is the energy of the dissociation of one chemical bond and n_{atoms} is the current number of the chemical bonds between counterpart's surfaces.

Using (6), one can find the total energy ($U_{TotalvdW}$) dissipated by van der Waals bonds

$$U_{TotalvdW} = n_{vdW}\, U_{vdW} \tag{6}$$

where U_{vdW} is the energy of the dissociation of a van der Waals bond, n_{vdW} is the current number of the vdW bonds within the contacting (overlapping) regions of the adhesive subscale. This energy is different at each time moment along the contact cycle due to variability of the number of nanoasperity in touch at that point. The energy spent for elastic deformation ($U_{elastic}$) of a nanoasperity or the elastic interlocking between the counterpart's surfaces of the silicon microgears teeth is also taken into the account. Hence, the total energy loss is

$$U_{diss=}\, U_{Totalchem} + U_{TotalvdW} + U_{elastic} \tag{7}$$

Then it follows from (4) and (7) that the friction force can be calculated as

$$F_f = (U_{Totalchemical} + U_{TotalvdW} + U_{elastic})/x \quad (8)$$

The numerical simulations show that $U_{Totalchem}(t)$ gives the greatest contibution to the sliding friction force in (7), and in turn in friction while $U_{TotalvdW}$ calculated by (6) gives roughly less than 40% of the total energy loss [21, 22]. Using ideas of Derjaguin [32], COF (the coefficient of friction) μ can be calculated as

$$\mu = F_f/(F_N + F_{adh}) \quad (9)$$

Hence, it follows from the above expression and (8) that COF is

$$\mu = U_{diss}/x(F_N + F_{adh}) \quad (10)$$

Here F_N is the nominal normal force applied to the tooth surface in the contact zone, and F_{adh} is the force of adhesion between contacting surfaces. Hence, the equation (10) can be rewritten as

$$\mu = U_{chemical}/(F_N + F_{adh})\ x + U_{vdW}/(F_N + F_{adh})\ x + U_{elastic}/(F_N + F_{adh})\ x \quad (11)$$

As it has been mentioned, the mechanisms caused the energy lost in the vacuum environment may be reduced to the energy lost due to the elastic interlocking between the asperities located on the meshing micro-tooth surfaces and the dissociation of chemical and van der Waals bonds, and this is reflected in the following formula for the coefficient of friction

$$\mu = \mu_{chemical} + \mu_{vdW} + \mu_{elastic} \quad (12)$$

Adhesion force for one nano-asperity is assumed as the pull-off force estimated by the Boussinesq-Kendall model modified by non-slip coefficient (C_{NS}) introduced [33-35]. Let F_{adh1} be the adhesion force of one nanoasperity and n be the number of asperities in contact. Then one has

$$F_{adh1} = \sqrt{8\,\pi\, w_{12}\, E^* C_{NS}\, a^3}. \quad (13)$$

Here w_{12} is the work of adhesion and a is the radius of the contact. For silicon, the Hamaker constant $A_{12} = 1.1 \times 10^{-18}\, J$ and the separation distance $D_0 = 1.49$ Å respectively [36], hence, the work of adhesion is calculated as

$$w_{12} = A_{12}/12\,\pi\, D_0^2 = 1.31\, J/m^2 \quad (14)$$

It is assumed that a is the half width of the silicon adhesive asperity, therefore, $a = W_{adhesive}/2 = 97.5\, nm$, then, by using Equation (13) and (15), the total adhesion force F_{adh} at each point over the sliding distance can be calculated as

$$F_{adh} = n\, F_{adh1} \quad (15)$$

The contact modulus for silicon gears can be calculated by substitution the corresponding values of Young's $E = 161\ GPa$, and the Poisson's ratio $\nu = 0.23$ [35, 37], hence, it is

$$E^* = E/2\,(1 - \nu^2) = 85.15\ GPa \quad (16)$$

The no-slip coefficient [33-35] can be found as

$$C_{NS} = \ (1 - \nu)\, ln(3 - 4\,\nu)/(1 - 2\,\nu)\ = 1.044. \quad (17)$$

Adhesion layer thickness was assumed according to Maugis approach (see for details [23]). Therefore, the asperities of both the atomic and adhesive sub-nanoscales will jump into contact when they are within this layer of adhesion. The contribution of the vdW interactions is twofold: (i) a small amount of energy is lost due to breaking vdW bonds, and (ii) these interactions may attract the counterpart and, therefore, to increase the number of interacting atomic subscale asperities that may greatly contribute to the amount of dissipated energy.

Thus, according to the roughness studies described above, a real silicon rough surface has been described at different scales: nanoscale that include atomic subscale of active chemical interactions and molecular subscale of active van der Waals interactions, and bulk elastic scale. The Borodich-Savencu (B-S) one level model [23-25] that have been developed for modelling of friction between nominally flat surfaces, has been extended to mirror the specific features of interactions between MEMS teeth. The B-S model assumed the gap between the

surfaces is constant, while the gap in a gear MEMS pair is changing during the mesh cycle. This was taken into account by the iterative solutions of two-dimensional frictional Hertz-type problems using the Cardiff numerical solver. The 2D Cardiff contact solver has been modified because the original solver was developed for EHL contact [27-29], while we consider the case when there is no lubricant. The modified solver and the above described approach allowed us to model tribology of curved teeth using nanoblocks consisting of atomic and molecular subscales located at varying levels. The apparent friction force and coefficient of friction μ have been calculated by estimations of the total energy per unit length dissipated through the above-mentioned physical and chemical mechanisms. It has been shown that there is a high possibility of stiction (cohesion or the so-called cold welding) between pure silicon MEMS teeth. Therefore, it has been proposed to functionalize the tooth surfaces by carbon-based monomolecular films.

SAMs have been widely proposed and characterised as the lubricants for MEMS [1-3]. These monomolecular films can decrease the COF and wear if they are deposited on the silicon substrate [38-40].The COF for the OTS-SAM functionalized coating over the silicon microgear MEMS tooth surface has been calculated for fully functionalized tooth surface, as shown in Figure 8 and second when the wear started to occur by stiction or due to the operation process (see [22] for details). The numerical simulations [22, 23] showed that the static coefficient of friction decreases from 0.85 for silicon to 0.2 for self-assembled monomolecular layer microgear MEMS teeth surfaces (Figure 5). The higher reduction in the coefficient of friction when applying the OTS-SAM is due to uniformity and higher packing density of the monomolecular layer along with the non-reactiveness of the terminal groups. For bare silicon, stick-slip maybe occurs due to cohesion or so-called cold welding between silicon contact surfaces, but this phenomenon has been completely eliminated by the OTS-SAM functionalized coated layer.

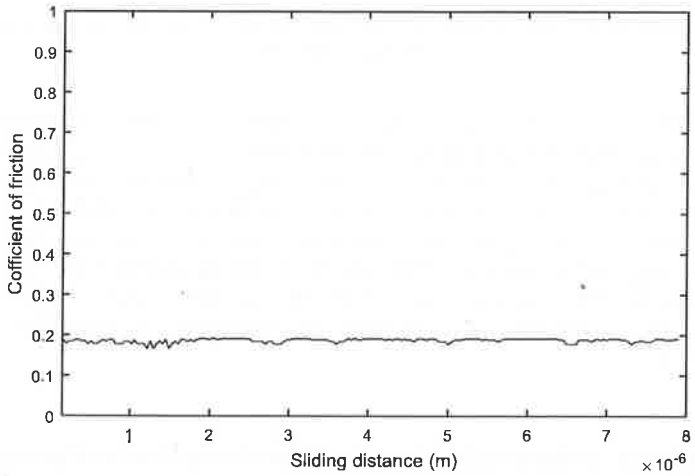

Figure 5. Numerical results on variation of COF for functionalised coating teeth surface by OTS– SAM layer [22].

When the microgear MEMS tooth surface has fully protected with OTS-SAM coating layer, the value of the COF is approximately 0.185. This value is quite suitable to continue the operating system without any problems occurring due to stiction or friction. As it has been mentioned above, this observation confirms our assumption that the temperature effects may be neglected for MEMS having functionalized protective monolayers.

Speaking about fatty acid monomolecular boundary layers, Akhmatov [41] noted that a new phase surface formed by CH_3 end-groups of carbon chains appear on the crystal surface. In the case under consideration, instead of the CH_3 end-groups of carbon chains we have the OTS-SAM that are charged due to uniform orientation of their molecules [9]. Let us consider two functionalized coated surfaces having the same charge. If these surfaces approach each other then, the boundary layer forces occur between the charged surfaces. The closer surfaces the higher boundary layer forces. Because these forces are repulsive, they generate extra negative pressure between these surfaces [41, 42]. In other words, the two functionalized surfaces will repel each other because they have the same charge [43, 44]. Due to this repulsion, possibility of stiction between these contacting functionalized surfaces is rather low. Due to lack of reliable experimental results, we have not taken into account the forces arose due to formation of the boundary layers between the coated surfaces. However, if one looks at the structure of a SAM layer where the head group is attached to the silicon surface due to chemical sorption, while the tails (spacer and terminals groups) are organised into regularly oriented molecular structure, then, it is very likely that the functionalized layers form charged boundary layers. Due to similar charged tails,

the boundary layer interactions between the SAM layers are repulsive; this will lead to decrease the value of the compression between surfaces, i.e. if the compressing normal force F_N is considered as positive then

$$F_N + F_{adh} < F_N.$$

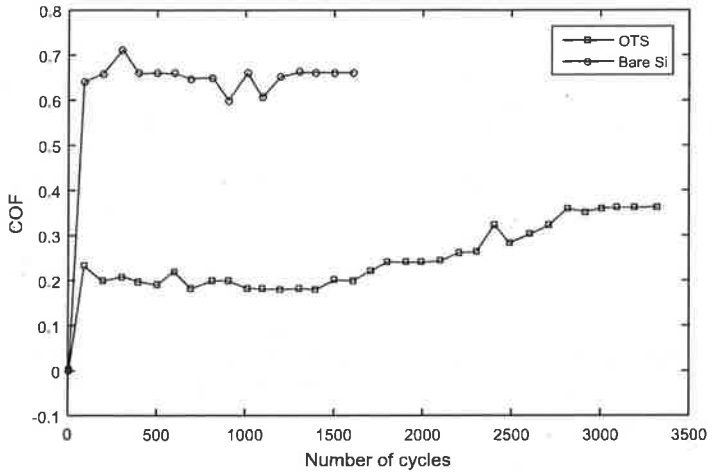

Figure 6. Experimental results on variation of COF with sliding cycles for bare Si and OTS at a sliding velocity of 2cm/sec and normal load of 5gm [45].

Here F_{adh} is the boundary layer repulsive force. Hence, the approach between the surfaces decreases and in turn, both values of the total energy dissipated by van der Waals bonds: $U_{TotalvdW}$ and the energy spent for elastic deformation of a nanoasperities or the elastic interlocking between the counterpart's surfaces $U_{elastic}$ will decrease. This will lead to general decrease of the coefficient of friction (COF). In addition, the functionalized layers prevent silicon surfaces from chemical interactions, therefore the energy dissipated by chemical bonds may be neglected. These phenomena can be the reason that the COF for OTS-SAM layer that has calculated from our model is 0.2, while it is about 0.075 for 50gm and sliding velocity 0.1mm/sec. However, for velocity equal to 2 cm/sec and load equal to 5gm, our estimations are quite close to the experimental observations (see Figure 6) [45].

3. Damage mechanics of carbon-based functionalised monomolecular layers

3.1 Classical models of damage accumulation.

The damage mechanics [46], has been well developed for bulk materials. Rabotnov has introduced an internal damage variable ω ($0 \leq \omega \leq 1$), while Kachanov worked with continuity variable ψ ($\psi = 1 - \omega$). If ω= 0 then the material is undamaged, if ω= 1 then the material is completely damaged. The damage variable ω is very important to study damage evolution of materials. It has been shown that often the use of the parameter is physically justified and it provides a measure of the influence that is randomly distributed micro defects exert on the macro parameters of a structure and its macro response [47].

The concept of damage has various applications [46-48] including tribological ones. Goryacheva and Chekina [49] developed a model of damage accumulation and fatigue wear within an elastic half-space. Contact of limited number of asperities with elastic half-space was considered by Goryacheva and Dobychin [50]; they obtained non-uniform load distribution between asperities. Various models of discrete contact were developed and described in detail by Goryacheva [51]. These models were used in various damage accumulation models of tribology including tribology of coated surfaces [19, 20].

A wide range of surface coatings materials were produced especially those based on carbon and other coating materials [52-54]. These coatings materials have the ability to work as solid lubricants and also as anti-wear coatings in different industrial and research applications. Besides they provide relatively low friction, these materials provide a very high resistance to wear and fracture. Normally, when the load applied, high shear stress

is generating on the surface and it may induce cracking process in the coating layers [55]. The crack growth is classified into two mechanisms. First, the failure in the interface between coating layer and substrate and the second is increasing of crack size or the growth of cracks through the coating layer itself. Both mechanisms of micro-cracks growth are governed by shear stress. The actual cracking mode depends upon the fracture strength of the coating material, interface strength, aspect ratio (ratio of the coating layer thickness to the radius of the circular shaft bar), and the elasticity of both coating and substrate materials. Moreover, in the cracked coated surface, the interfacial stresses close to the crack tip can simulated similar to the free edge stresses that have extensively studied in laminated composite materials [55]. In 2003 Goryacheva and Torskaya introduced a model for calculation the damage accumulation in a coated surface in friction contact [56]. The calculations were performed by applying a periodic system of indenters. These calculations are based on development of models of discrete contact described by Goryacheva [49]. Later the models of the damage accumulation in coated surfaces were developed further by taking into account the effects of the surface geometry parameters at the microscale on the performance of the sliding contact pressure and the sub-stresses in the coating layer joined to an elastic surface [19, 20]. Here the damage accumulation will be considered in application to monomolecular coatings.

3.2 Distribution of contact forces between atomic scale asperities

A carbon-based functionalized coating material has been used in this model, which is molecular ultra-thin layers organized by one layer of molecules assembled on silicon substrate (see Figure 7).

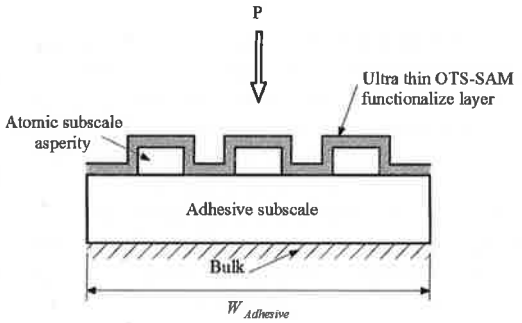

Figure 7. A nanoblock functionalized by carbon-based monomolecular layer.

In Fig. 7 $W_{adhasive}$ is the width of the adhesive subscale of the nanoblock coated by ultra-thin monomolecular layer. Therefore, the elastic properties of this layer such as elasticity moduli and the Poisson ratios are not taken into the account. Through the sliding motion of the microgear teeth upon each other, the blocks of asperities generate some friction force. This will cause a destruction of the surface functionalized coating after some contact cycles. As it follows from the above description of the damage model presented, it is important that the functionalized layer is very thin and the stress distributions of the non-functionalized and functionalized tooth surfaces differ due to the difference in the COF, while specific properties of the OTS-SAM are taken into account through the critical value of the damage parameter. Thus, the damage model presented in this paper is applicable to other thin carbon-based functionalized layers. The same is related to the influence of the packing density and the ordering of SAMs, i.e. these specific properties are also taken into account through the critical value of the damage parameter.

Figure 8 shows the approximation of the asperities geometry by the atomic subscale of the nanoblock.

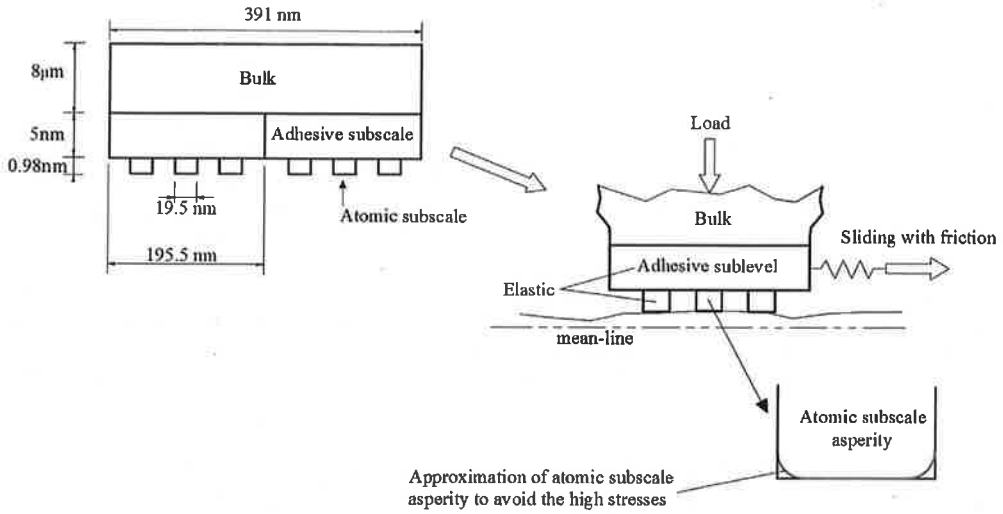

Figure 8. Approximation of geometry shape for the atomic subscale asperities

Here we intend to determine the load distribution between atomic-scale asperities. Then we will analyze solutions of the appropriate contact problems. The analysis is possible due to some assumptions. First, we assume that the nanoscale asperities deform only elastically due to the Polonsky-Keer effect [57, 58]. We assume also that the shear stresses within the contact regions may be neglected. Because the SAM coatings are very thin (in fact, they are monomolecular coatings), the mechanical properties of the coating do not influence the contact characteristics and the coating surface stresses can be considered as equal to the stresses on between tooth surfaces. The study of this problem consists of the following steps: (i) determination of load distribution between atomic asperities taking into account mutual effect; (ii) calculation of friction force; (iii) contact problem solution for single atomic asperity, calculation of stresses at the surface taking into account friction; (iv) analysis of damage accumulation for time-dependent load.

For the first step of the solution, we assume that contact pressures under the flat asperities are constant. The scheme of multiple contacts is presented in Figures 7 and 8.

We consider that the condition of equal penetration is valid for the center of each asperity:

$$w_i = c = const, \quad i = 1 \dots 9 \tag{18}$$

The elastic displacements are determined by deformation of asperities $w_i^{(1)}$ and elastic half-space $w_i^{(2)}$:

$$w_i(x,y) = w_i^{(1)}(x,y) + w_i^{(2)}(x,y), (x,y) \in \Omega_i, \quad i = 1 \dots 9 \tag{19}$$

where Ω_i is a contact zone for an asperity. The model of Winkler-Fuss foundation is used for asperities, the compliance K_s is obtained from silicon elastic characteristics (the silicon Young modulus is $E_s = 161\, GPa$ [37]) and the heights of atomic and adhesive asperities (see Figure 3):

$$w_i^{(1)}(x,y) = K_s p_i, \quad i = 1 \dots 9 \tag{20}$$

Here p_i is a constant pressure in a contact zone i. The surface displacement of the elastic half-space under a constant load distributed in circle region is determined by the following relation for the centre of the region [59]:

$$w_i^{(2)}(x,y) = \sum_{j=1}^{9} \frac{4(1-\upsilon^2)p_j}{E_s} \varphi(r_i^j), \tag{21}$$

$$\varphi(r_i^j) = \begin{cases} a & i = j \\ \frac{r_i^j}{\pi}\left(E\left(\frac{a}{r_i^j}\right) - \left(1 - \left(\frac{a}{r_i^j}\right)^2\right)K\left(\frac{a}{r_i^j}\right)\right) & i \neq j \end{cases} \tag{22}$$

Here $E(x), K(x)$ are elliptic integrals, r_i^j is the distance between the centres of zones i and j.

The equilibrium condition is used as following:

$$P = \sum_{i=1}^{9} P_i \tag{23}$$

Here P_i is a load for an asperity.

In above relations we have linear dependence of displacements on constant pressures inside the contact zones, so the problem reduces to a system of linear equations:

$$\begin{bmatrix} k_v + k_1^1 & k_1^2 & \cdots & k_1^9 & -c \\ . & . & . & . & . \\ . & . & . & . & . \\ k_9^1 & k_9^2 & \ldots & k_v + k_9^9 & -c \\ 1 & 1 & \ldots & 1 & 0 \end{bmatrix} \times \begin{bmatrix} P_1 \\ . \\ . \\ P_9 \\ 1 \end{bmatrix} = \begin{bmatrix} 0 \\ . \\ . \\ 0 \\ P \end{bmatrix} \tag{24}$$

Here k_v is load-displacement coefficient, i.e. the Winkler-Fuss elastic bed constant (deformation of asperity), k_j^i is influence coefficient caused by deformation of the counter body. The results are obtained for six different values of loading that have choosing for single adhesive asperity. The results for load distributions between atomic-scale asperities are presented in the following table:

Table 1 Nominal and distributed load over the atomic subscale asperities

Load for adhesive asperity, $\times 10^{-6}\ N$	Corner asperity, $\times 10^{-6}\ N$	Side asperity, $\times 10^{-6}\ N$	Central asperity $\times 10^{-6}\ N$
0.817	0.0963	0.0884	0.0782
0.99	0.1167	0.1071	0.0947
1.794	0.2115	0.1941	0.1717
3.428	0.4041	0.3709	0.3281
4.405	0.5193	0.4766	0.4216
7.017	0.8275	0.7595	0.6719

The maximal and minimal values of the load are realized for the corner and central asperities respectively.

3.3 Calculation of surface stresses at each atomic scale asperity.

The geometry shape of the atomic subscale asperities have approximated to semicircular cross-section to avoid the high stresses on the edges of the asperities. The geometry surface shape has approximated according to the following shape function $f(r) = B_4 r^4$ with degree of order 4 to be close to its original shape. Therefore, it is look similar to an indenter with flat base and semicircular edges. The geometrical parameter B_4 has calculated to be equal to $4 \times 10^{22}\ m^{-3}$ for the geometry of atomic asperities.

To show the effect of approximation especially close to the edge, the shift distance could be calculated from power law as follow

$$z = f(r) = B_4\ r^4 \tag{25}$$

Then by using the half width of one atomic subscale asperity as $(r) = 9.75 \times 10^{-9}$, and $B_4 = 4 \times 10^{22} m^{-3}$ Then, $z = 4 \times 10^{22} m^{-3} \times (9.75 \times 10^{-9})^4$, that is mean, $z = 3.62 \times 10^{-10} = 3.62$ Å. Therefore, the atomic subscale asperity edge will be shifted by z , which is approximately distance of two atoms, that is relatively small distance but in the same time rapidly reduce the stresses on the edges of the asperity. We use Galin's solution [60] to find contact pressure distribution:

$$p(r) = \frac{E^*}{4\pi^2}\int_0^{2\pi}\int_0^a \Delta f(\rho)\frac{arctg\left(\frac{\sqrt{a^2-r^2}\sqrt{a^2-\rho^2}}{\sqrt{r^2-2r\rho cos\alpha+\rho^2}}\right)}{\sqrt{r^2-2r\rho cos\alpha+\rho^2}}\rho d\rho d\alpha,\ E^* = \frac{E_s}{2(1-\upsilon^2)} \quad (26)$$

The equilibrium condition is the following:

$$P = \int_0^{2\pi}\int_0^a p(r) r dr d\varphi \quad (27)$$

The problem is solved numerically. Iterations are used to satisfy equilibrium conditions and to find contact radius a. The loads values obtained from the multiple contact problem solution have been used to determine the contact pressures. The principal shear stress at the sliding contact surfaces are calculated using generalized Boussinesq and Cerruti solutions [59] with $\mu = 0.2$ (see Figure 5). For the edge of the atomic subscale asperity, the results for maximal load $0.8275221560 \times 10^{-6}\ N$ are presented in Figure 9a for contact pressure and Figure 9b for principal shear stress τ at the surface of atomic subscale asperity. The radius of contact is $8.95\ nm$. It is important to note that the procedure of calculations with power 6 in (22), i.e. $z = B_6\ r^6$, leads to a very similar result; in particular, the difference in maximal value of pressure and the contact radius is less than 8%.

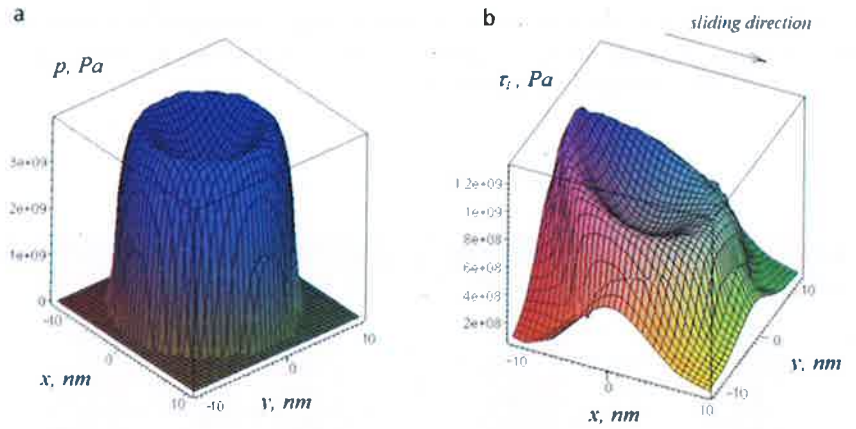

Figure 9. (a) Contact pressure for atomic subscale asperity; (b) principal shear stress τ at the surface of atomic subscale asperity.

Simulations have showed that the atomic subscale asperity, which is located at the corner of the adhesive subscale asperity, is under stresses higher than stresses at other asperities. Because of that, the cracks or damage in the functionalized coating layer will begin in the edge of the asperity. Figure 9b shows clearly that there is high principle shear stress on the edge of the adhesive subscale asperity (at the corner atomic subscale asperity), which gives damage a high chance to start there. That is maybe explained why the coatings fracture occurs not simultaneously. The results of calculations for contact area are in the following table:

Table 2 Nominal load and the radius of contact area over the atomic subscale asperities

Load for adhesive asperity, $\times 10^{-6}\ N$	Corner asperity, nm	Side asperity, nm	Central asperity, nm
0.817	5.82	5.72	5.59
0.99	6.05	5.94	5.80
1.79	6.82	6.70	6.52
3.43	7.76	7.62	7.44
4.41	8.16	8.02	7.82
7.02	8.95	8.80	8.59

3.4 Calculation of the damage accumulation

The relation between the damage accumulation rate and the amplitude value $\Delta\tau_1$ of the principal shear stress at the point can be presented as the following modification of the Rabotnov equation:

$$\dot{\omega}(x,t) = \frac{\partial\omega(x,t)}{\partial t} = c \cdot (\Delta\tau_1(x,t))^m \tag{28}$$

Where c and m are phenomenological parameters and $\Delta\tau 1(x,t)$ is the amplitude value of the principal shear stress at the point (x) for one period of sliding loading. The parameter c is used to normalise the equation. Indeed, the physical dimensions of the components are the following:

$$[\dot{\omega}] = T^{-1};\ [\Delta\tau_1] = FL^{-2};\ [(\Delta\tau_1)^m] = (FL^{-2})^m;\ [c] = (FL^{-2})^{-m}T^{-1} \tag{29}$$

where F, L and T are the dimensions of force, length and time respectively. Here we have used the Maxwell notation $[\cdot]$ for physical dimension of the variable in the square brackets. If the problem is periodic, then we can replace the time variable by the number of cycles N.

Now we have to estimate the number of subcycles k that is how many times we can observe increasing and decreasing of the load acting on the nanoblock within one cycle for MEMS teeth

$$\dot{\omega}(x,k) = c \cdot (\Delta\tau_1(x,k))^m \tag{30}$$

The equation (30) can be transformed to an equation for damage $\omega(x,k)$, which is accumulated at fixed point x during k subcycles of a mesh cycle in a nanoblock

$$\omega(x,k) = \sum_{i=1}^{k} c_1 \cdot (\Delta\tau_{1i}(x,k))^m \tag{31}$$

Where c_1 is a normalization parameter such that the damage $\omega(x,k)$ calculated according to (31) satisfies the restrictions $(0 \leq \omega \leq 1)$. The physical dimension of c_1 is

$$[c_1] = (FL^{-2})^{-m} \tag{32}$$

Using the numerical simulations [22], we obtained the graph of the distribution of pressure acting on a tooth along x (sliding distance). Distribution of pressure acting on a tooth along sliding distance are shown in Figure 10. According to the pressure distribution over sliding distance, there are $k = 48$ fluctuation cycles of pressures.

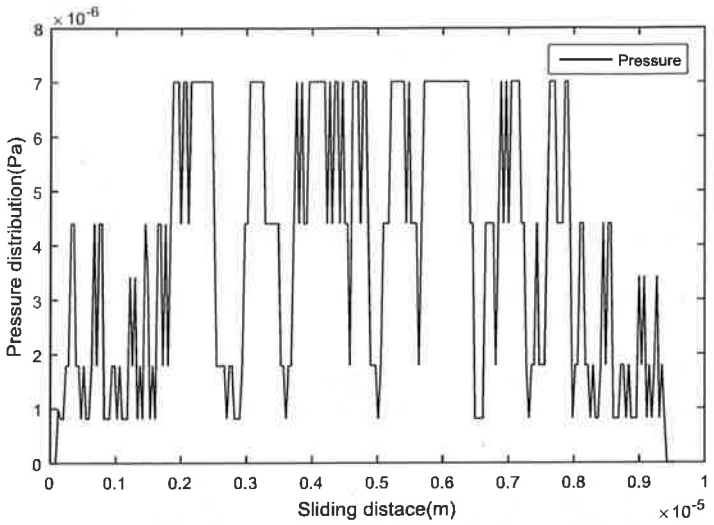

Figure 10. Distribution of pressure acting on a tooth along x (sliding distance). There are k=48 picks of the pressure fluctuations.

Because each nanoblock at the atomic subscale has 9 asperities, 9 different values of the principal shear stress $\Delta\tau_1$ acting on each atomic asperity are calculated using the distribution of pressure obtained. To show the principal shear stress distributions, the cross-sections in sliding direction through the center of contact zone for each of the atomic asperity of a nanoblock are taken. These stresses are presented below for the corner atomic subscale asperity (line 1), side atomic subscale asperity (line 2) and central atomic subscale asperity (line 3). Load for an adhesive subscale asperity is $7.016 \times 10^{-6} N$ (maximum) as shown in Figure 11.

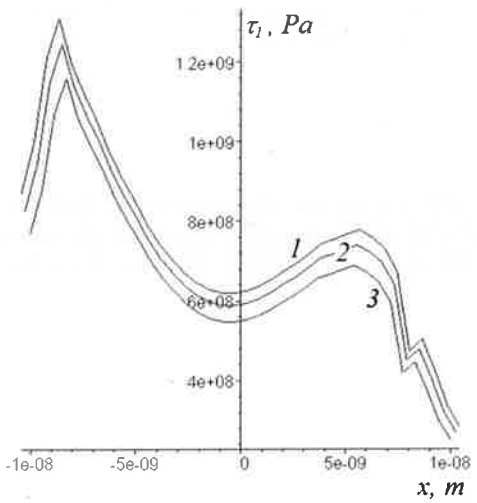

Figure 11. Principal shear stress distributions for corner (1), side (2) and central atomic subscale asperities (3) when load is maximum 7.016×10^{-6} N.

Figure 12 shows principal shear stress distributions for the corner atomic subscale asperity, when it under the effect of different values of loads applied for example ($0.816 \times 10^{-6} N$, $3.428 \times 10^{-6} N$ and $7.016 \times 10^{-6} N$ for 1, 2, 3 lines respectively).

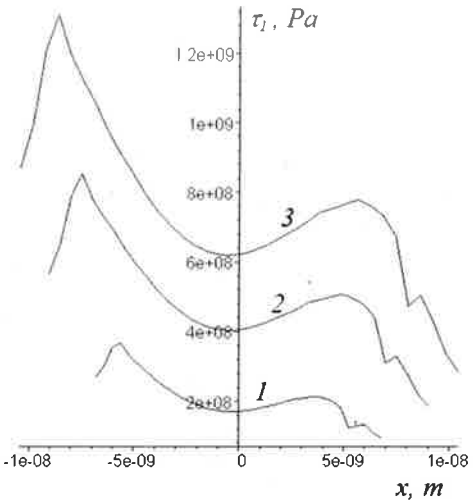

Figure 12. Principal shear stress distributions for the corner atomic subscale asperity with different values of load ($0.816 \times 10^{-6} N$, $3.428 \times 10^{-6} N$ and $7.016 \times 10^{-6} N$ for lines 1, 2 and 3 respectively.

The numerical results for damage function (ω/c_1) has been calculated with two different value for the phenomenological parameter m (obtained for $m = 1$ and $= 2$) the summation of 48 cycles, the corner atomic subscale asperity (line 1), side atomic subscale asperity (line 2) and central atomic subscale asperity (line 3). One can see that the variations of the parameter m cause the significant difference between the graphs. One can see in Figure 11 that the maximum value for damage function (ω/c_1) equals (2.4×10^{10}) when $m = 1$. While it equals to (1.6×10^{19}) when $m = 2$ as shown in Figures 13 and 14 respectively.

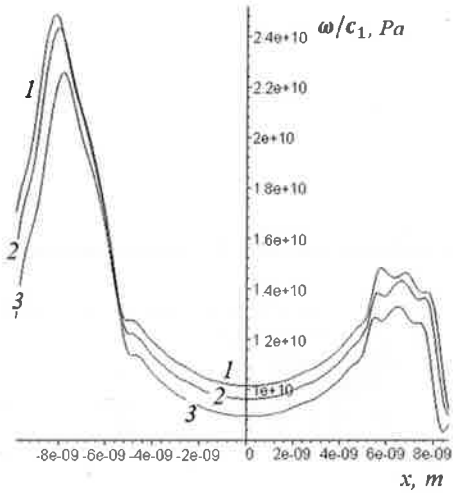

Figure 13. Damage function (ω/c_1) when m=1, corner atomic subscale asperity (line 1), side atomic subscale asperity (line 2) and central atomic subscale asperity (line 3) respectively.

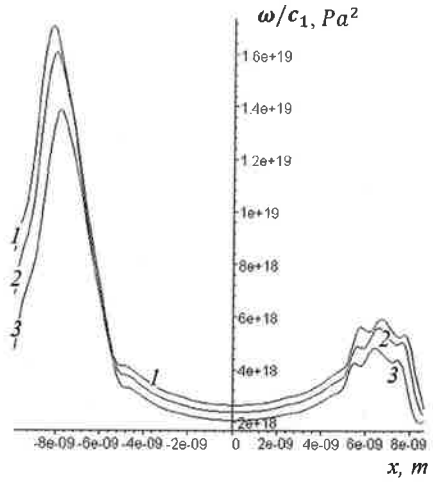

Figure 14. Damage function (ω/c_1) when m=2, corner atomic subscale asperity (line 1), side atomic subscale asperity (line 2) and central atomic subscale asperity (line 3) respectively.

The maximum values for the damage function (ω/c_1) have been calculated with respect to their location on the microgear MEMS tooth surface and presented in Table 3 when the parameter $m = 1$ and in Table 4 when $m = 2$. This calculations for corner atomic subscale asperity, side atomic subscale asperity and central atomic subscale asperity respectively to show the variation of damage with respect to location of subscale asperity.

Table 3 Maximum values for ω/c_1 when m=1 and their location:

Asperity position	x	ω/c_1
Corner asperity	-0.8226×10^{-8}	0.2482×10^{11}
Side asperity	-0.8007×10^{-8}	0.2433×10^{11}
Central asperity	-0.78×10^{-8}	0.2257×10^{11}

Table 4 Maximum values for ω/c_1 when m=2 and their location:

Asperity position	x	ω/c_1
Corner asperity	-0.8182×10^{-8}	0.1706×10^{20}
Side asperity	-0.7990×10^{-8}	0.1608×10^{20}
Central asperity	-0.78×10^{-8}	0.1388×10^{20}

That is mean the lifetime cycle of the corner atomic subscale asperity, which is located at the edge of the adhesive subscale asperity where the shear stress at maximum value, will be less than the lifetime of central

atomic subscale asperity by 9% when $m = 1$ and 18.65% when $m = 2$. In other words, the start of coating fracture is at the point of maximal damage concentration.

After the damage parameter reaches its critical value, the fracture process within the coating (wear of the monomolecular coating) may have two main scenarios: (i) the full instantaneous delamination of the coating from a single atomic scale asperity of the nanoblock; and (ii) the partial delamination of the coating at the periphery of the atomic scale asperity. The former scenario may get a realization if the interactions between the spacer groups of the monomolecular layer are considerably higher than the chemisorption bonds between the heads and the substrate (see Figure 1). The later scenario may get a realization if the chemisorption bonds are rather strong and the interactions between the spacer groups are relatively weak. The realization of the later scenario leads to higher life expectation of the functionalized layer.

Conclusion

In this paper, the work of microgear MEMS teeth have been simulated in the vacuum environment and, therefore, the energy dissipation mechanisms have been reduced to the dissociation of chemical and van der Waals interactions along with the elastic interlocking between counterparts subscale asperities. The models developed allowed us to simulate various tribological phenomena, including adhesion, friction, wear and the elastic interlocking of the tooth surfaces.

The chemically active tips of bare silicon asperities are terminated by self-assembled monomolecular layer of Octadecyltrichlorosilane ($CH_3\ (CH_2)_{17}SiCl_3$, *OTS*). This layer not only prevent teeth from cold welding (creating chemical bonds) between silicon surfaces but also the functionalized coating layers form charged boundary layers. Due to similar charged tails, the boundary layer interactions between the self-assembled monomolecular layers are repulsive; this will lead to decrease the value of the compressing force. Therefore, for the same normal force F_N the approach of the surface will decrease and hence, both values of $U_{TotalvdW}$ and $U_{elastic}$ will decrease. This will lead to general decrease of the COF.

The rough MEMS tooth roughness has been described as smooth curved silicon surfaces covered by adhesive nanoblocks representing the asperities. Each nanoblock consists of two hierarchical atomic and adhesive subscale elements. The amount of energy dissipated by different physical and chemical mechanisms in additional to the sliding contact motion between the counterparts can be estimated and used to evaluate the frictional force. Numerical simulations show that if the microgear MEMS surfaces are not functionalized, then the friction force is very high [12, 13]. For the functionalized MEMS, initially the tooth surfaces do not stick to each other. However, as the functionalized monomolecular layer starts to be worn away, the stiction may occur.

To study the wear of the functionalized coating, the model of damage accumulation that connects contact stresses and strength characteristics of materials with fatigue crack initiation [10, 11], was adapted for this specific case. For the present composition of structure, we are interested only in surface damage because the strength characteristics are essentially different for the functionalized carbon-based monomolecular layer and bulk silicon. The dry frictional contact of a single tooth pair has been studied because the maximum damage occurs under action of the maximum load.

The damage evolution is described for several levels of external load. It is shown that the coatings wear occurs not simultaneously, because the atomic subscale element located at the corner of the nanoblock will have higher stresses than other atomic subscale elements of the nanoblock. It is argued that after the damage parameter reaches its critical value, the wear process within the coating (wear of the monomolecular coating) may have two main scenarios: (i) the full instantaneous delamination of the coating from a single atomic scale asperity of the nanoblock; and (ii) the partial delamination of the coating at the periphery of the atomic scale asperity. The former scenario may get a realization if the interactions between the spacer groups of the monomolecular layer are considerably higher than the chemisorption bonds between the heads and the substrate (see Figure 1). The later scenario may get a realization if the chemisorption bonds are rather strong and the interactions between the spacer groups are relatively weak. The realization of the later scenario leads to higher life expectation of the functionalized layer.

Funding

The authors are grateful to the Leverhulme Trust for financial support of the collaboration between the authors within the CARBTRIB International Network. The work was also partially supported by Russian Foundation for

Basic Research (projects No. 17-01-00352 and 16-08-00749). In addition, the Iraqi Ministry of Higher Education and Scientific Research that is gratefully acknowledged, supported the studies of one of the authors (Nabeel Almuramady) at the Cardiff School of Engineering. Thanks are also due to the University of Al-Qadisiyah for their support of the studies.

Acknowledgments

The authors are also grateful to Professor H.P. Evans, Dr. O. Savencu and Dr. S. Khaustov (Cardiff School of Engineering) for their valuable comments.

References

[1] Ghodssi R and Lin P eds. MEMS Materials and Processes Handbook. Springer Science and Business Media; 2011

[2] Gad-el-Hak M ed. The MEMS Handbook. CRC press; 2002

[3] Tanner DM, Smith NF, Irwin LW et al. MEMS reliability: infrastructure, test structures, experiments, and failure modes. No. SAND2000-0091. Sandia National Labs., Albuquerque, NM (US); Sandia National Labs., Livermore, USA; 2000

[4] Maboudian R, Shurst WR and Carraro C. Tribological challenges in micromechanical systems. Tribology Letters 2002; 12: 95-100.

[5] Maboudian R and Howe RT. Critical review: Adhesion in surface micromechanical structures. Journal of Vacuum Science & Technology B: Microelectronics and Nanometer Structures Processing, Measurement, and Phenomena 1997; 15(1):1-20.

[6] Zhang WM, Yan H, Peng ZK and Meng G. Electrostatic pull-in instability in MEMS/NEMS: A review. Sensors and Actuators A: Physical 2014;214:187-218.

[7] Fonseca DJ and Sequera M. On MEMS reliability and failure mechanisms. International Journal of Quality, Statistics, and Reliability 2011. doi:10.1155/2011/820243

[8] Iannacci J. Reliability of MEMS: A perspective on failure mechanisms, improvement solutions and best practices at development level. Displays 2015; 37:62-71.

[9] Ulman A. An Introduction to Ultrathin Organic Films: From Langmuir-Blodgett to Self-Assembly. Academic Press; 2013

[10] Jabbarzadeh A. Friction anisotropy and asymmetry in self assembled monolayer. Tribology International 2016; 102: 600-607.

[11] Masuko M, Miyamoto H, Suzuki A. Tribological characteristics of self-assembled monolayer with siloxane bonding to Si surface. Tribology International 2007; 40: 1587-1596.

[12] Cui B, Zhang J, Chen J. Tribological properties of poly(amide amine) and small molecule composite self-assembled monolayers: Influence of functional group of small molecule. Tribology International 2013; 62: 149-154.

[13] Elinski, MB, Menard, BD, Liu, ZT, Batteas, JD Adhesion and friction at graphene/self-assembled monolayer interfaces investigated by atomic force microscopy. Journal of Physical Chemistry C 2017; 21: 5635-5641.

[14] Wang J, Zhang K, Wang FG, Zheng WT. Improving frictional properties of DLC films by surface energy manipulation. RSC Advances 2018; 8: 11388-11394.

[15] Sun, CG., Xia, D. S., Yu, Y., Zhang, H. C. Tribological properties of self-assembled monolayers prepared on titanium film. Materials Research Innovations 2015; 19: 919-923

[16] Nian J, Si Y, Guo Z. Advances in atomic-scale tribological mechanisms of solid interfaces. Tribology International 2016; 94: 1-13.

[17] Krivtsov AM and Morozov NF. On mechanical characteristics of nanocrystals. Physics of the Solid State 2002; 44: 2260-2265.

[18] Loboda OS, Krivtsov AM. The influence of the scale factor on the elastic moduli of a 3D nanocrystal. Mechanics of Solids 2005; 40: 20-32.

[19] Goryacheva IG and Torskaya EV. Modeling of fatigue wear of a two-layered elastic half-space in contact with periodic system of indenters. Wear 2010; 268(11):1417-22.

[20] Torskaya EV. Modeling of fatigue damage of coated bodies under frictional loading. Physical mesomechanics 2016;19(3):291-7.

[21] Almuramady N and Borodich FM. Adhesive Contact between Silicon-Based MEMS Tooth Surfaces Modelled by the Multiscale Multi-Block Model. International Journal of Advances on Automotive and Technology 2017; 1(2): 59-66.

[22] Almuramady N. Dry friction between rough surfaces of silicon and functionalized gear microelectromechanical systems. PhD thesis, Cardiff University; 2017.

[23] Borodich FM and Savencu O. Hierarchical models of engineering rough surfaces and bio-inspired adhesives. In: Heepe L, Xue L and Gorb S, editors. Bio-Inspired Structured Adhesives: Biological Prototypes, Fabrication, Tribological Properties, Contact Mechanics, and Novel Concepts. Springer; 2017, p. 179-219.

[24] Savencu O and Borodich FM. Modelling of friction using a structural multilevel hierarchical model of rough surfaces. Proc. NSCM-27: the 27th Nordic Seminar on Computational Mechanics, KTH, Stockholm; 2014, p. 136-9.

[25] Savencu O. Simulations of dry friction between rough surfaces and corresponding nonlinear problems at nano and microscales. PhD thesis, Cardiff University; 2016

[26] Maugis, D. Contact, *Adhesion and Rupture of Elastic Solids,* Berlin, Springer-Verlag Berlin Heidelberg, 2000.

[27] Evans HP, Snidle RW, Sharif KJ, Shaw BA and Zhang J. Analysis of micro-elastohydrodynamic lubrication and prediction of surface fatigue damage in micropitting tests on helical gears. Journal of Tribology 2013; 135(1):011501.

[28] Al-Mayali MF, Evans HP and Sharif KJ. Assessment of the effects of residual stresses on fatigue life of real rough surfaces in lubricated contact. In: Students on Applied Engineering (ISCAE), International Conference for IEEE; 2016, p. 123-8.

[29] Khaustov S. Elastohydrodynamic lubrication and surface fatigue modelling of spur gears over the meshing cycle. PhD thesis, Cardiff University; 2016.

[30] Brousseau E, Al-Musawi RS and Lebiez D. A hybrid roll-to-roll AFM set-up for high throughput tip-based nano-machining. Manufacturing Letters 2015; 6:10-13.

[31] Dean JA. Lange's Chemistry Handbook. University of Tennessee, Knoxville: McGrawHill, Inc; 1999.

[32] Derjaguin BV.. Molecular theory of friction and sliding. Zhurn. Phis. Khim (in Russian) 1934; 5:1165-72.

[33] Borodich FM. The Hertz-type and adhesive contact problems for depth-sensing indentation. Adv. Appl. Mech. 2014; 47: 225-366.

[34] Borodich FM and Keer LM. Evaluation of elastic modulus of materials by adhesive (no–slip) nano–indentation. In Proceedings of the Royal Society of London A: Mathematical, Physical and Engineering Sciences 2004; 460(2042): 507-514.

[35] Borodich FM. Contact problems at nano/microscale and depth sensing indentation techniques. Materials Science Forum, Trans Tech Publications, 2011; 662: 53-76.

[36] Tas N, Sonnenberg T, Jansen H, Legtenberg R and Elwenspoek M. Stiction in surface micromachining. Journal of Micromechanics and Microengineering 1996; 6(4):385.

[37] Teodorescu M, Theodossiades S and Rahnejat H. Impact dynamics of rough and surface protected MEMS gears. Tribology international 2009; 42(2):197-205.

[38] Lacks DJ and Levandovsky A. Effect of particle size distribution on the polarity of triboelectric charging in granular insulator systems. Journal of Electrostatics 2007; 65(2):107-112.

[39] Komvopoulos K. Surface engineering and microtribology for microelectromechanical systems. Wear 1996; 200(1-2):305-327.

[40] Spearing SM. Materials issues in microelectromechanical systems (MEMS). Acta materialia 2000; 48(1):179-96.

[41] Akhmatov AS Molecular Physics of Boundary Friction, GIFML, Moscow,1963. (English Transl. by Israel Program for Sc. Translations, Jerusalem, 1966).

[42] Pipes RB and Pagano NJ. Interlaminar stresses in composite laminates under uniform axial extension. In: Mechanics of Composite Materials, Springer, Netherlands; 1994, p. 234-45.

[43] Deryagin BV, Krotova NA and Smilga VP. Adhesion of Solids. Consultant Bureau, New York; 1978.

[44] Li D, Wang Y and Xia Y. Electrospinning nanofibers as uniaxially aligned arrays and layer-by-layer stacked films. Advanced Materials 2004; 16(4):361-6.

[45] Satyanarayana N, Sinha SK and Srinivasan MP. Friction and wear life evaluation of silane based self assembled monolayers on silicon surface. Tribology and Interface Engineering Series 2005; 48:821-6.

[46] Krajcinovic D. Damage Mechanics. Elsevier, 1996.

[47] Krajcinovic D. Constitutive equations for damaging materials. Journal of applied mechanics 1983; 50(2):355-60.

[48] Manoylov AV, Borodich FM and Evans HP. Modelling of elastic properties of sintered porous materials. Proc. R. Soc. London A: Mathematical, Physical and Engineering Sciences 2013; 469(2154): 2012.0689.

[49] Goryacheva IG, Chekina OG. Surface fatigue damage model, Soviet Journal of Friction and Wear 1990; 11(3):1–11.

[50] Goryacheva IG, Dobychin MN. Multiple contact model in the problems of tribo-mechanics. Tribology International 1991; 24(1):29-35.

[51] Goryacheva I. Contact Mechanics in Tribology. Dordrecht, Kluwer, 1998.

[52] Wang DF and Kato K. Nano-Scale Fatigue Wear of Carbon Nitride Coatings: Part I - Wear Properties. ASME Journal of Tribology 2003; 125(2):430–6.

[53] Wang DF and Kato K. Nano-scale fatigue wear of carbon nitride coatings: part II - Wear Mechanisms: ASME Journal of Tribology 2003; 125(2):437-44.

[54] Stewart S and Ahmed R. Rolling contact fatigue of surface coatings—a review. Wear 2002; 253(11):1132-44.

[55] Pipes, R.B. and Pagano, N.J., 1994. Interlaminar stresses in composite laminates under uniform axial extension. In Mechanics of Composite Materials, pp. 234-245. Springer Netherlands.

[56] Goryacheva IG and Torskaya EV. Stress and fracture analysis in periodic contact problem for coated bodies. Fatigue & Fracture of Engineering Materials & Structures 2003, 26(4):343-8.

[57] Polonsky IA and Keer LM. Scale effects of elastic-plastic behavior of microscopic asperity contacts. Journal of Tribology 1996; 118:335-40.

[58] Polonsky IA and Keer LM. Simulation of microscopic elastic-plastic contacts by using discrete dislocations. In Proceedings of the Royal Society of London A: Mathematical, Physical and Engineering Sciences 1996; 452(1953):2173-94.

[59] Johnson KL. Contact Mechanics, Cambridge: Cambridge University Press, 1985.

[60] Contact Problems. The legacy of L.A. Galin. Gladwell GML, editor. Springer, Netherlands, 2008.

Figure1

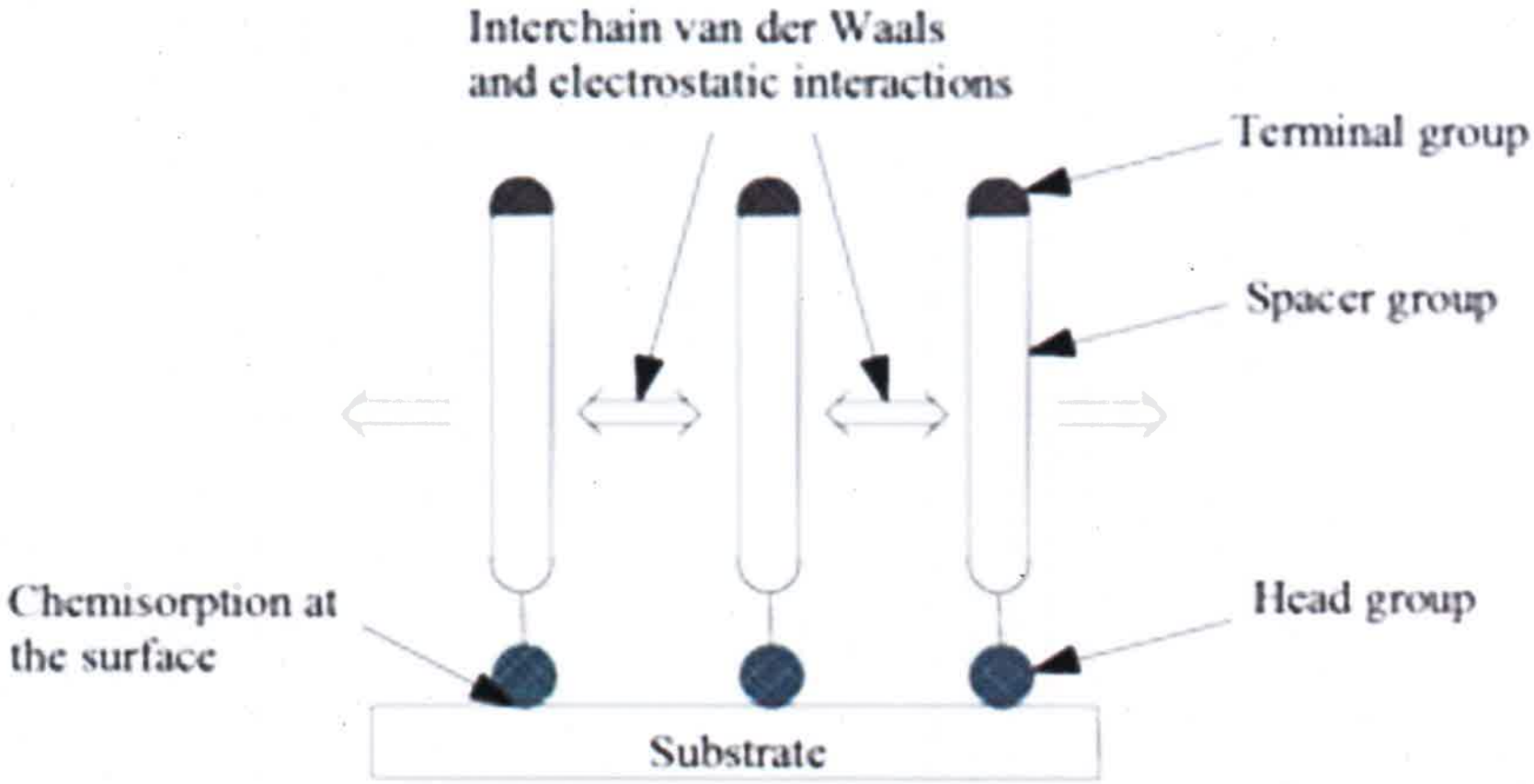
Interchain van der Waals
and electrostatic interactions
Terminal group
Spacer group
Chemisorption at
the surface
Head group
Substrate

Figure2

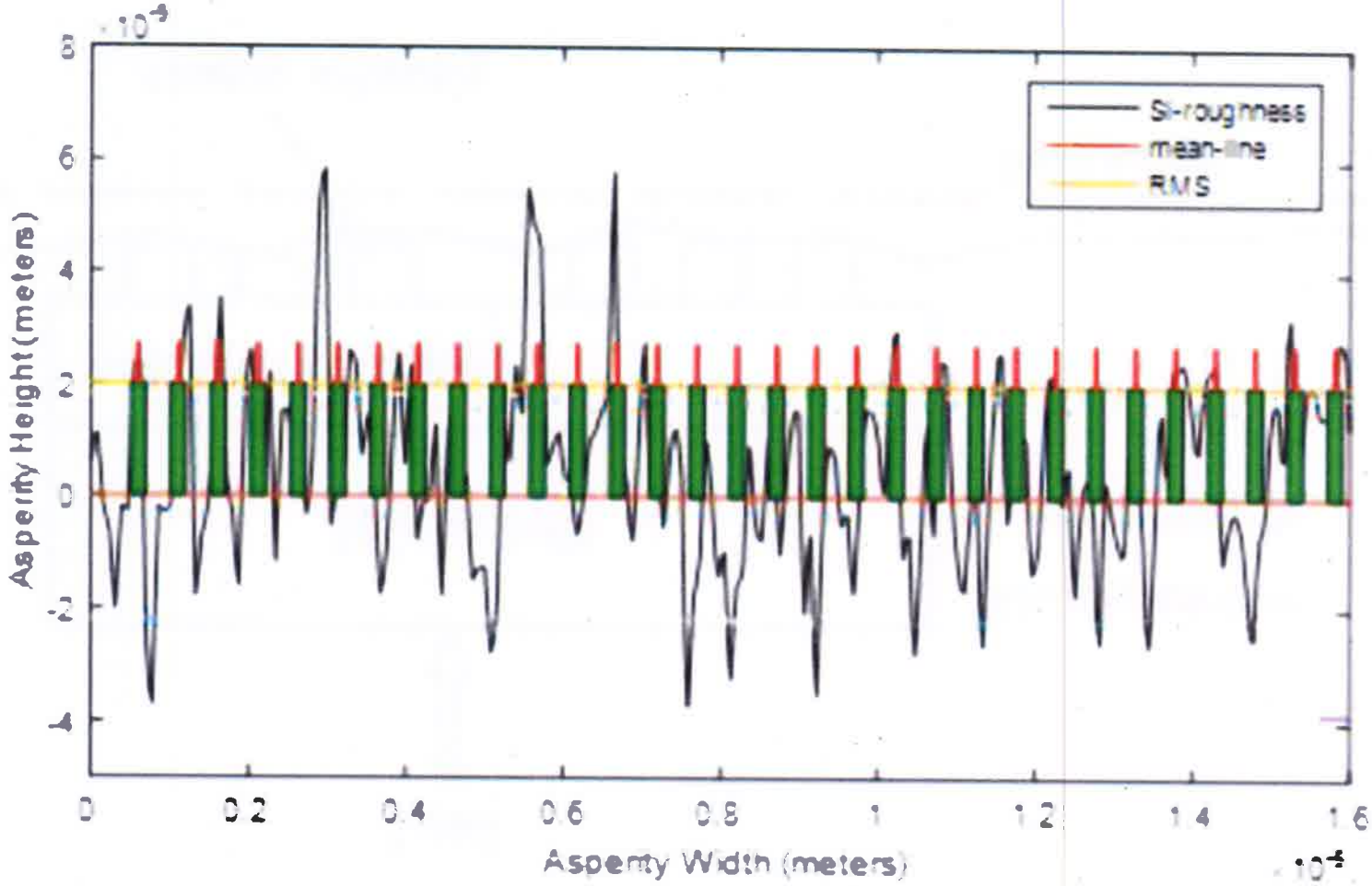
Si-roughness
mean-line
RMS
Asperity Height (meters)
Asperity Width (meters)
0
0.2
0.4
0.6
0.8
1
1.2
1.4
1.6

Figure3

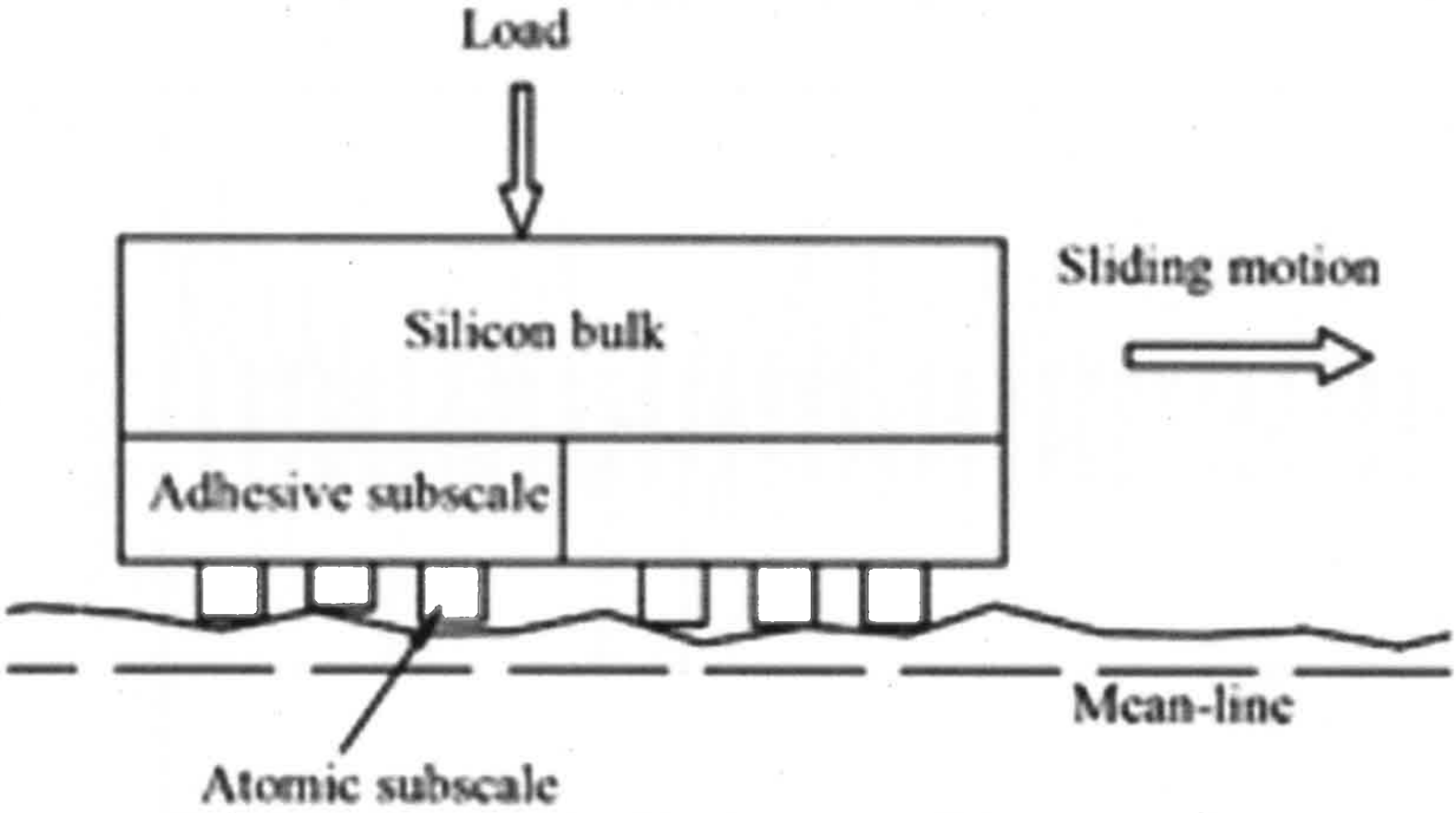
Load
Silicon bulk
Sliding motion
Adhesive subscale
Mean-line
Atomic subscale

Figure4

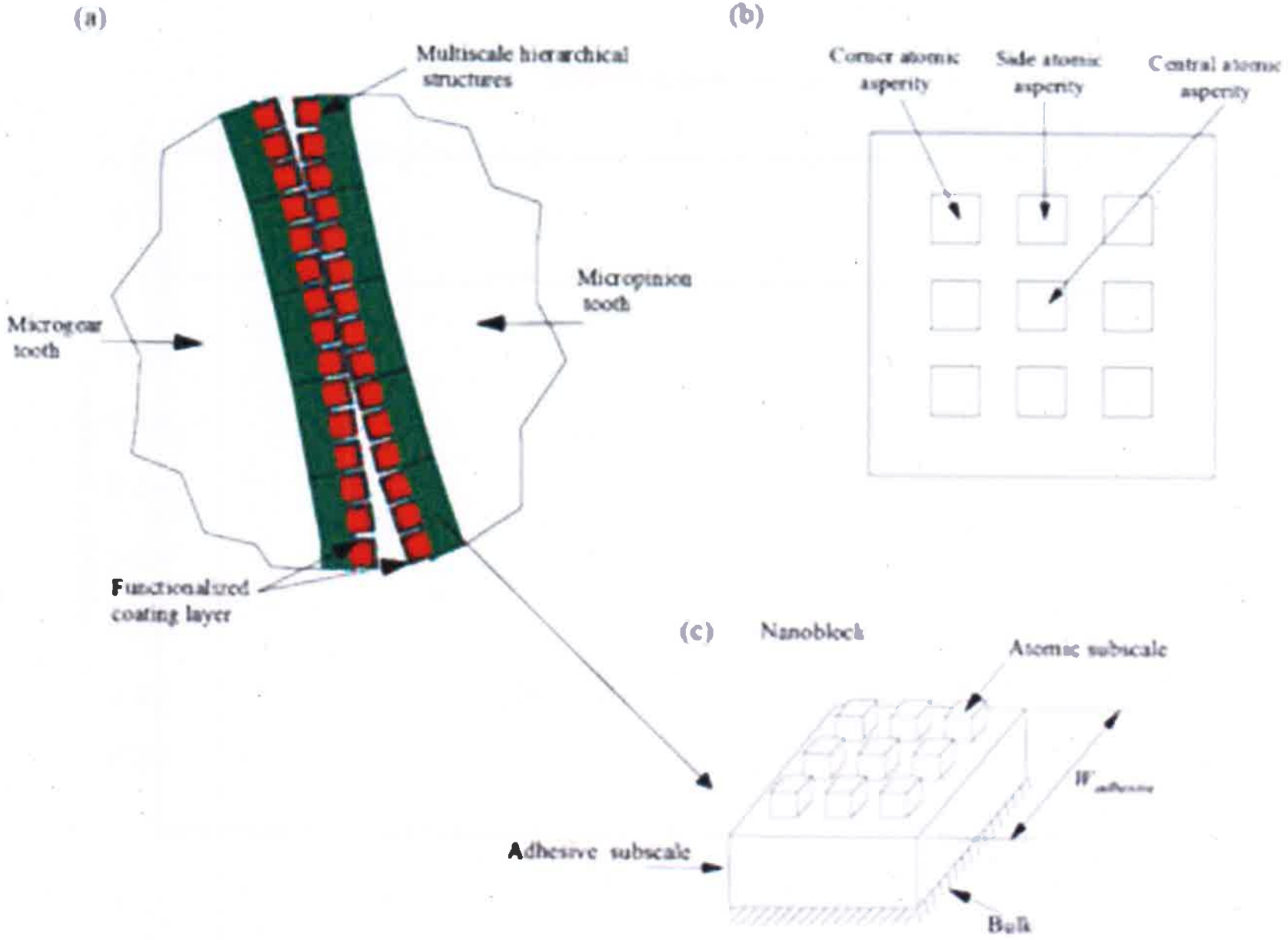
(a)
Multiscale hierarchical structures
Microgear tooth
Microgear tooth
Functionalized coating layer
(b)
Corner atomic asperity
Side atomic asperity
Central atomic asperity
(c)
Nanoblock
Atomic subscale
Adhesive subscale
Bulk

Figure5

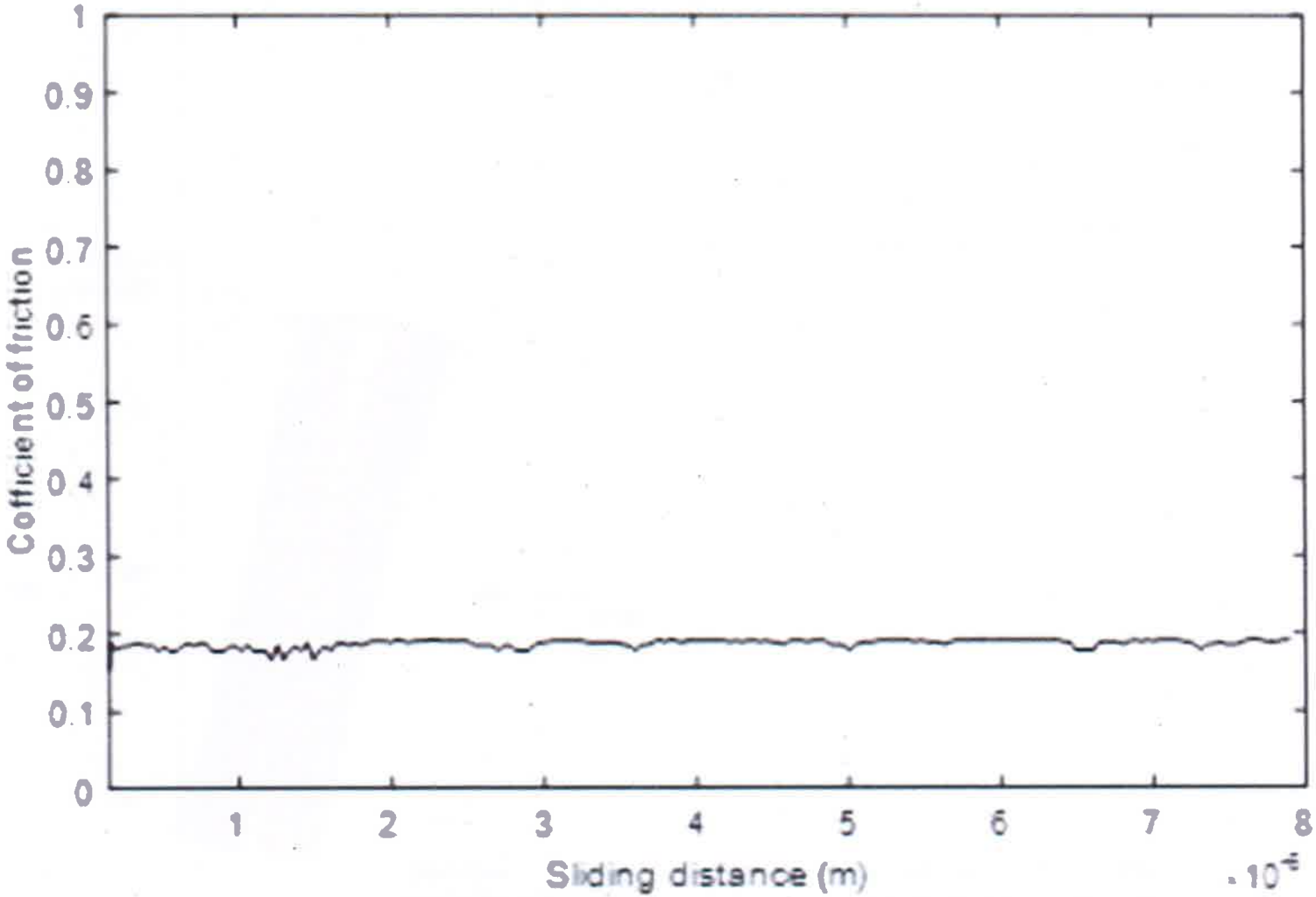
Cofficient of friction
0
0.1
0.2
0.3
0.4
0.5
0.6
0.7
0.8
0.9
1
1
2
3
4
5
6
7
8
Sliding distance (m)
$\cdot 10^{-6}$

Figure6

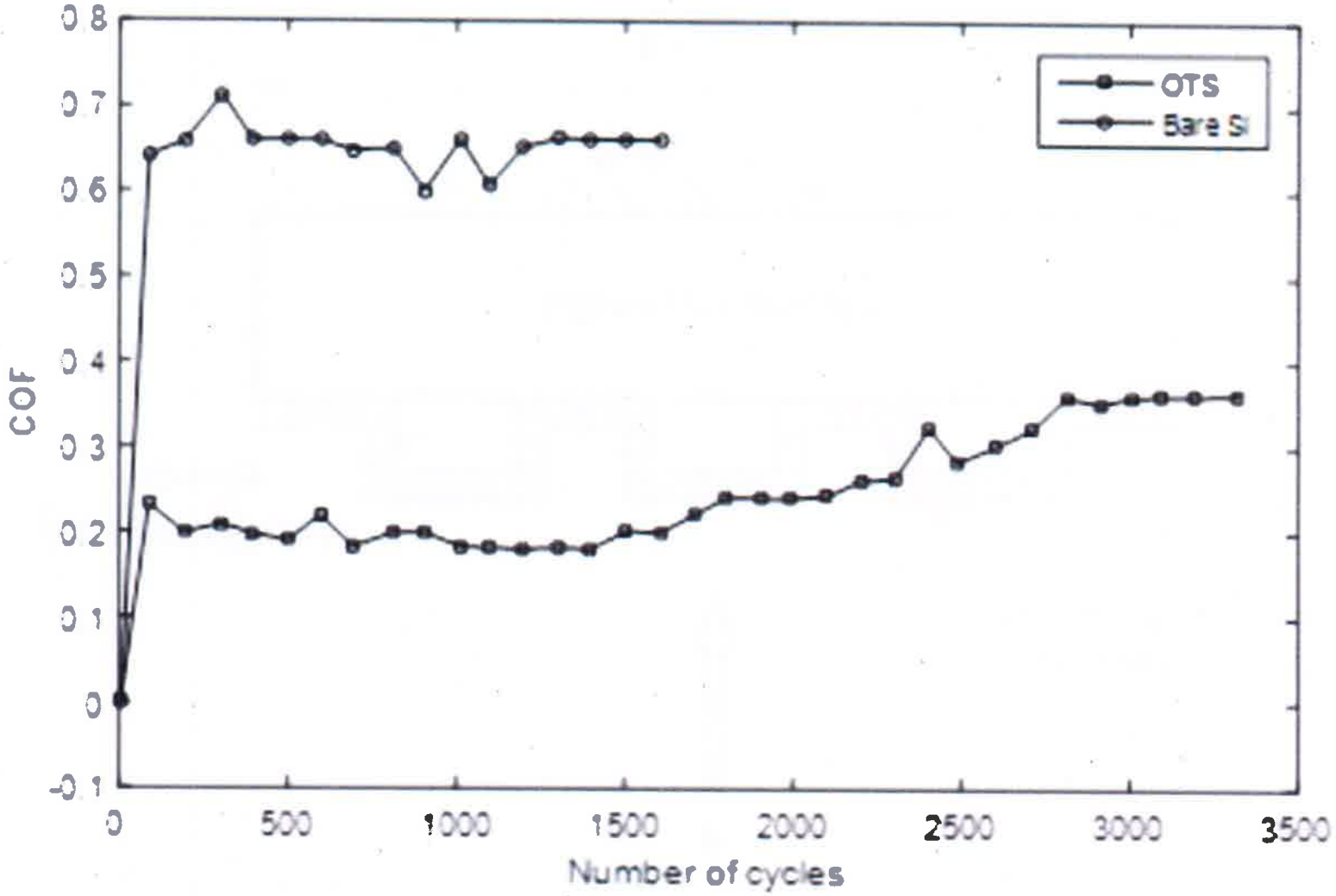
0.8
0.7
0.6
0.5
0.4
0.3
0.2
0.1
0
-0.1
COF
0
500
1000
1500
2000
2500
3000
3500
Number of cycles
OTS
Bare Si

Figure7

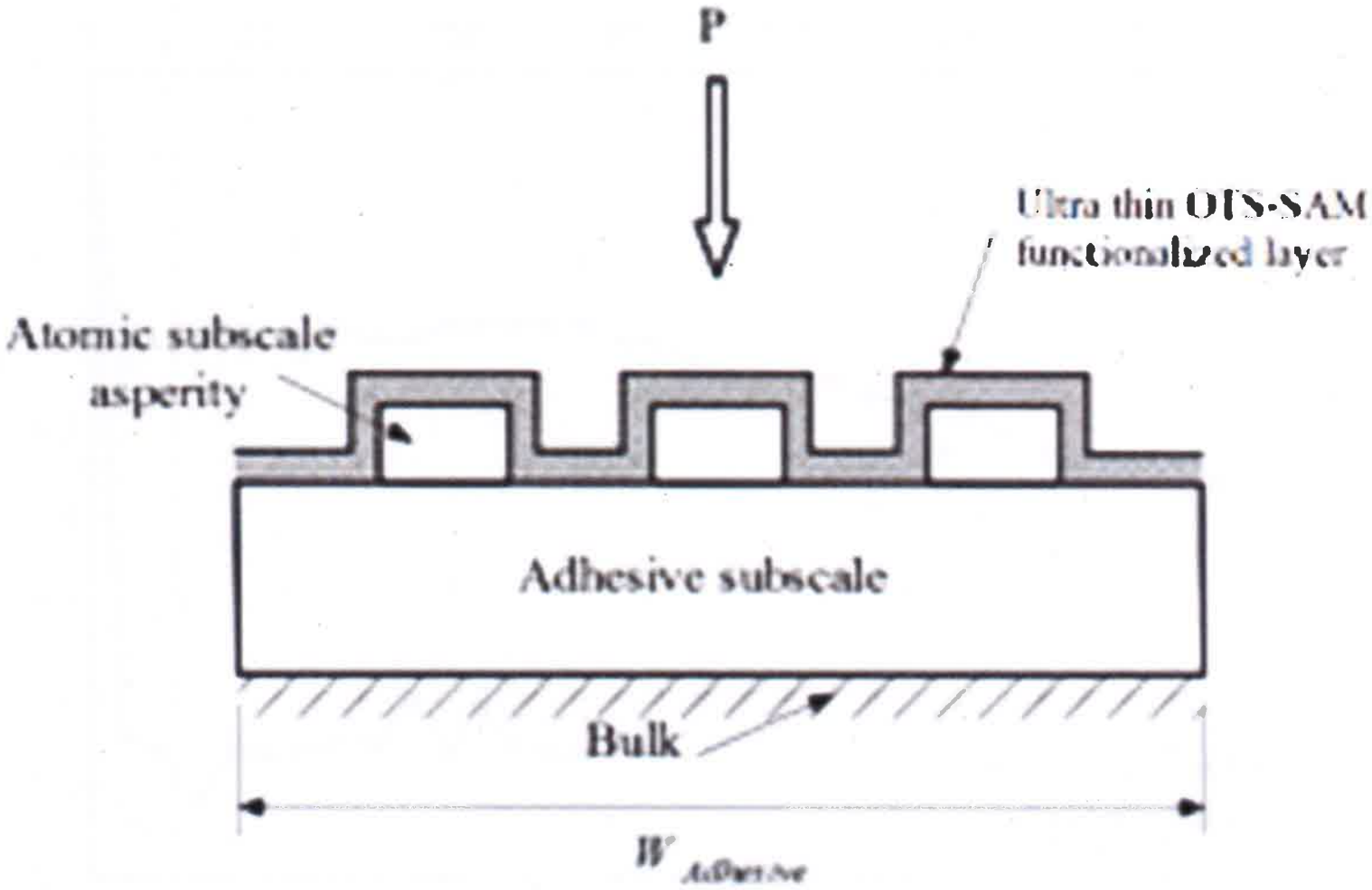
P
Ultra thin OTS-SAM
functionalized layer
Atomic subscale
asperity
Adhesive subscale
Bulk
W

Figure8

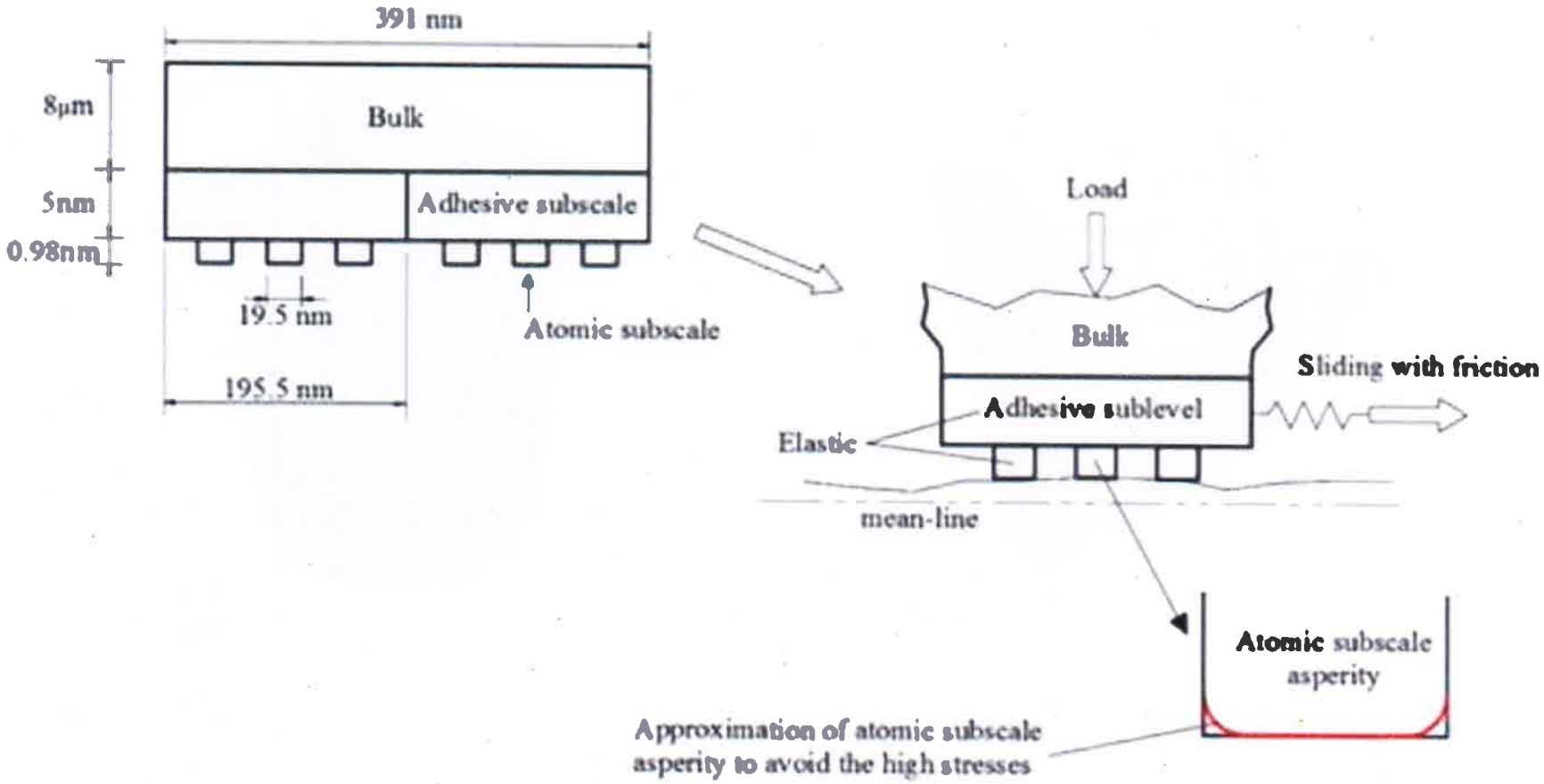
391 nm
8μm
Bulk
5nm
Adhesive subscale
0.98nm
19.5 nm
Atomic subscale
195.5 nm
Load
Bulk
Sliding with friction
Adhesive sublevel
Elastic
mean-line
Atomic subscale asperity
Approximation of atomic subscale asperity to avoid the high stresses

Figure9

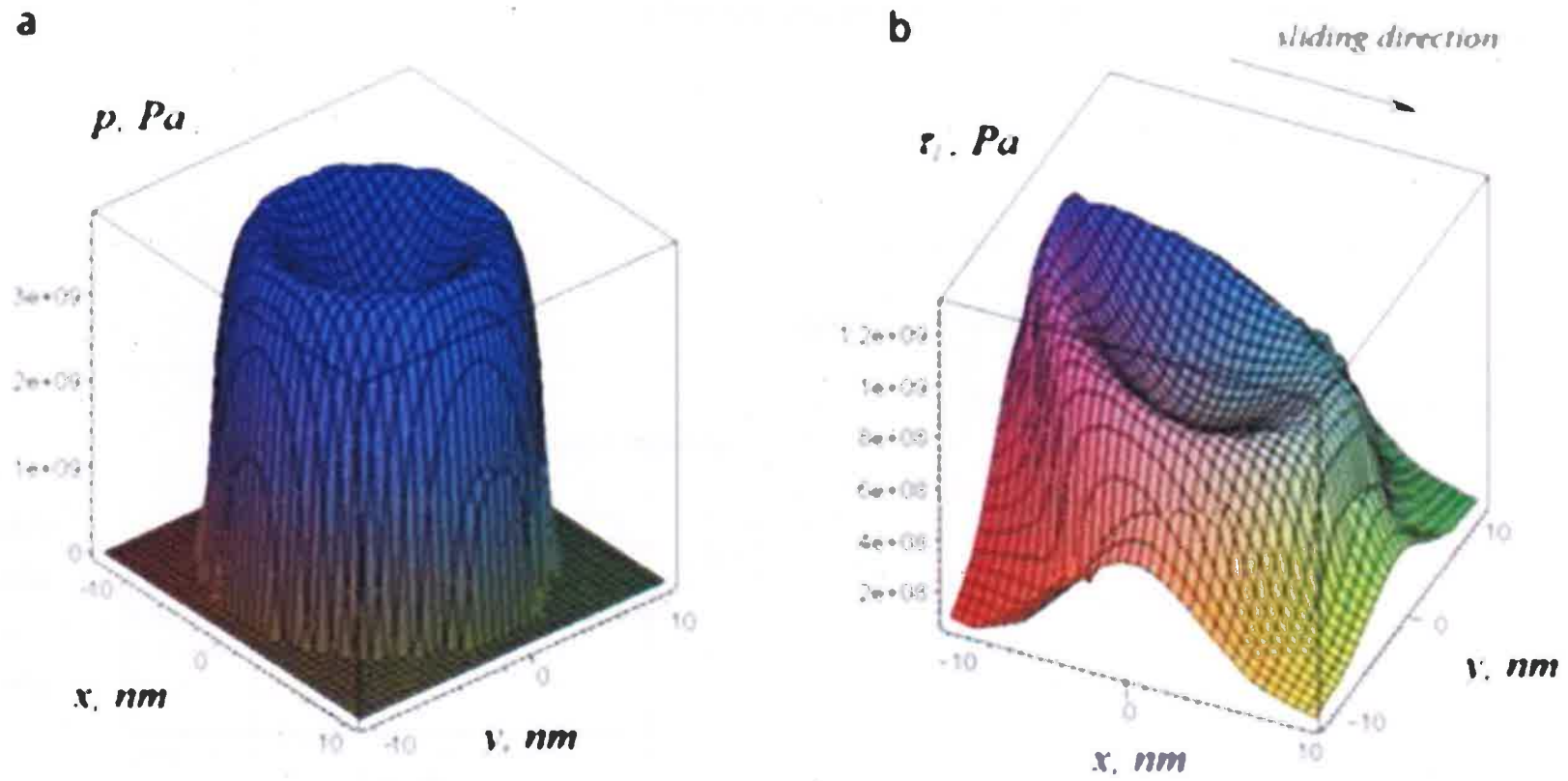
a
p, Pa
3e+09
2e+09
1e+09
0
-10
0
10
x, nm
-10
0
10
y, nm
b
sliding direction
τ, Pa
1.2e+09
1e+09
8e+08
6e+08
4e+08
2e+08
-10
0
10
x, nm
10
0
-10
y, nm

Figure10

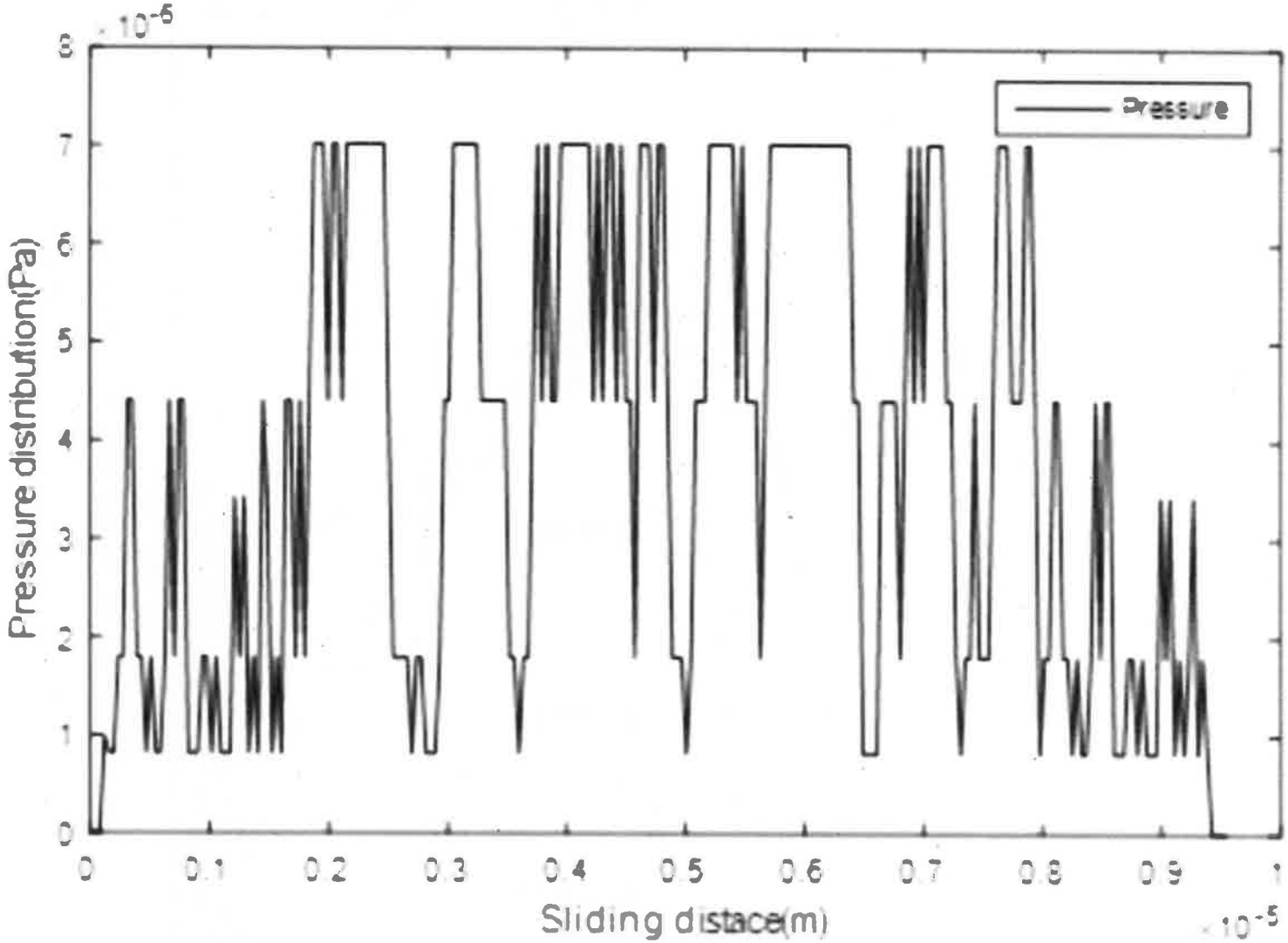
x 10^-6
8
7
6
5
4
3
2
1
0
Pressure distribution(Pa)
Pressure
0
0.1
0.2
0.3
0.4
0.5
0.6
0.7
0.8
0.9
1
Sliding distace(m)
x 10^-5

Figure11

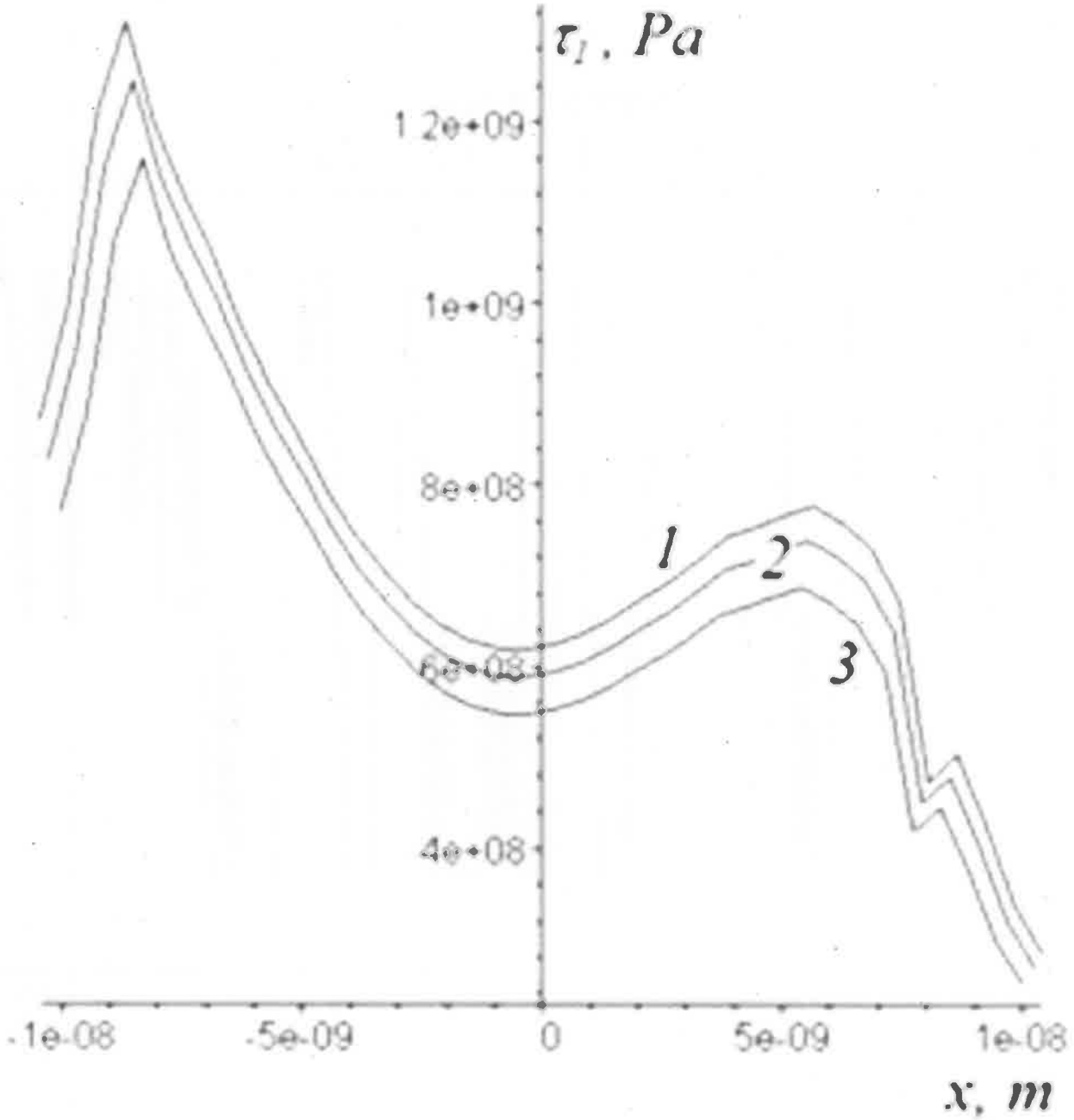

Figure12

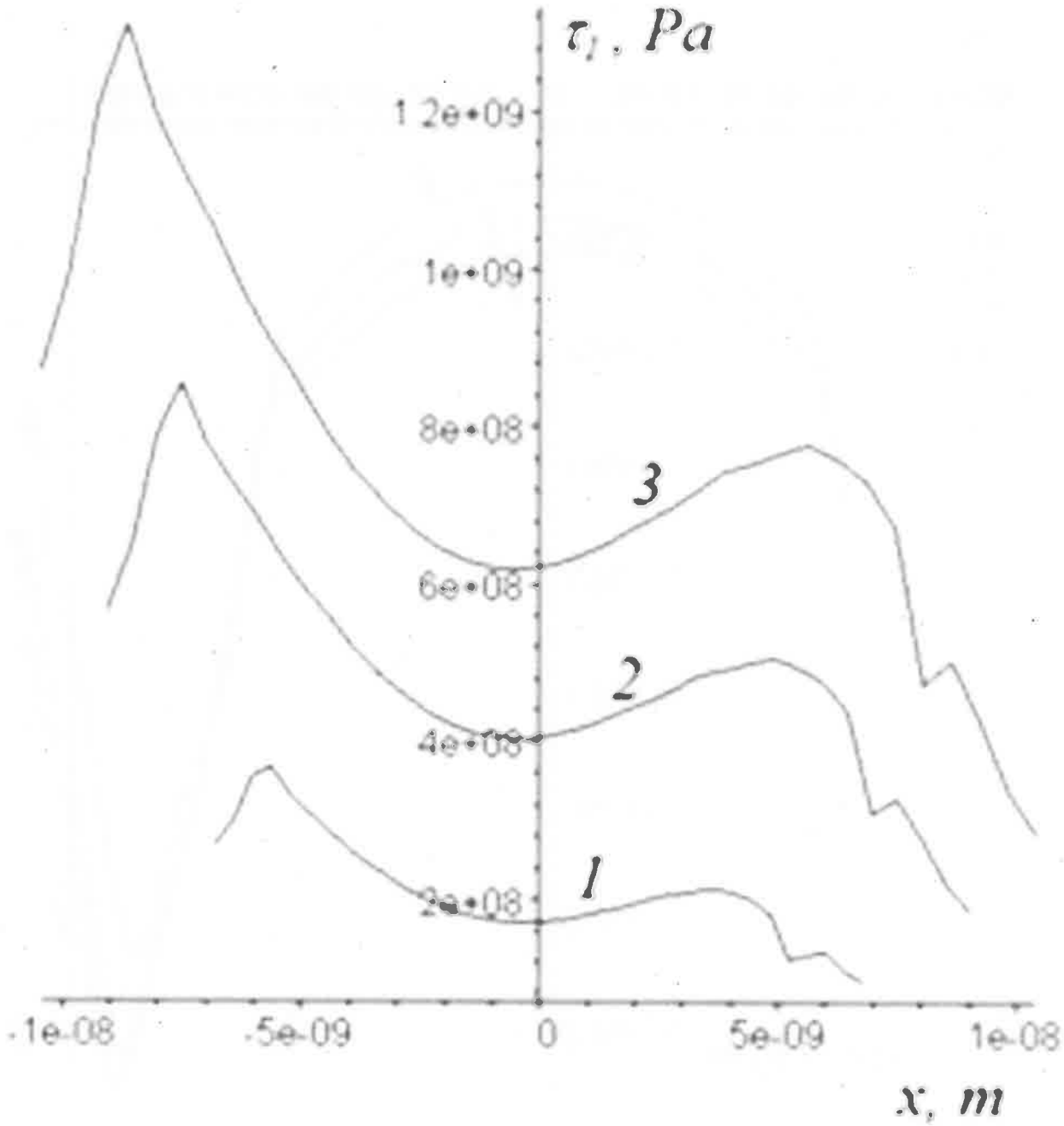
τ_l, Pa
1.2e+09
1e+09
8e+08
6e+08
4e+08
2e+08
3
2
1
-1e-08
-5e-09
0
5e-09
1e-08
x, m

Figure13

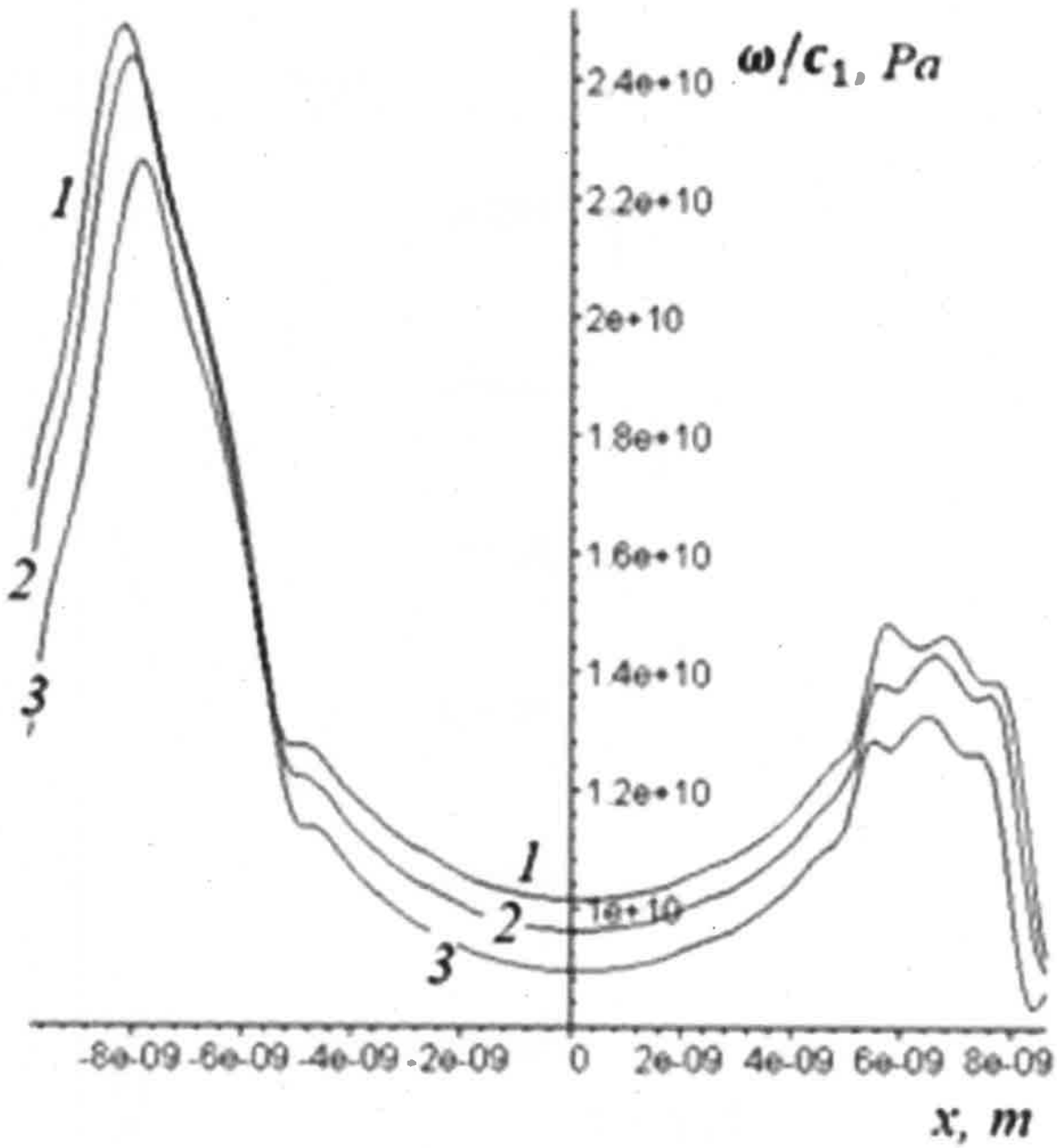
ω/c1, Pa
2.4e+10
2.2e+10
2e+10
1.8e+10
1.6e+10
1.4e+10
1.2e+10
1e+10
1
2
3
-8e-09 -6e-09 -4e-09 -2e-09 0 2e-09 4e-09 6e-09 8e-09
x, m

Figure14

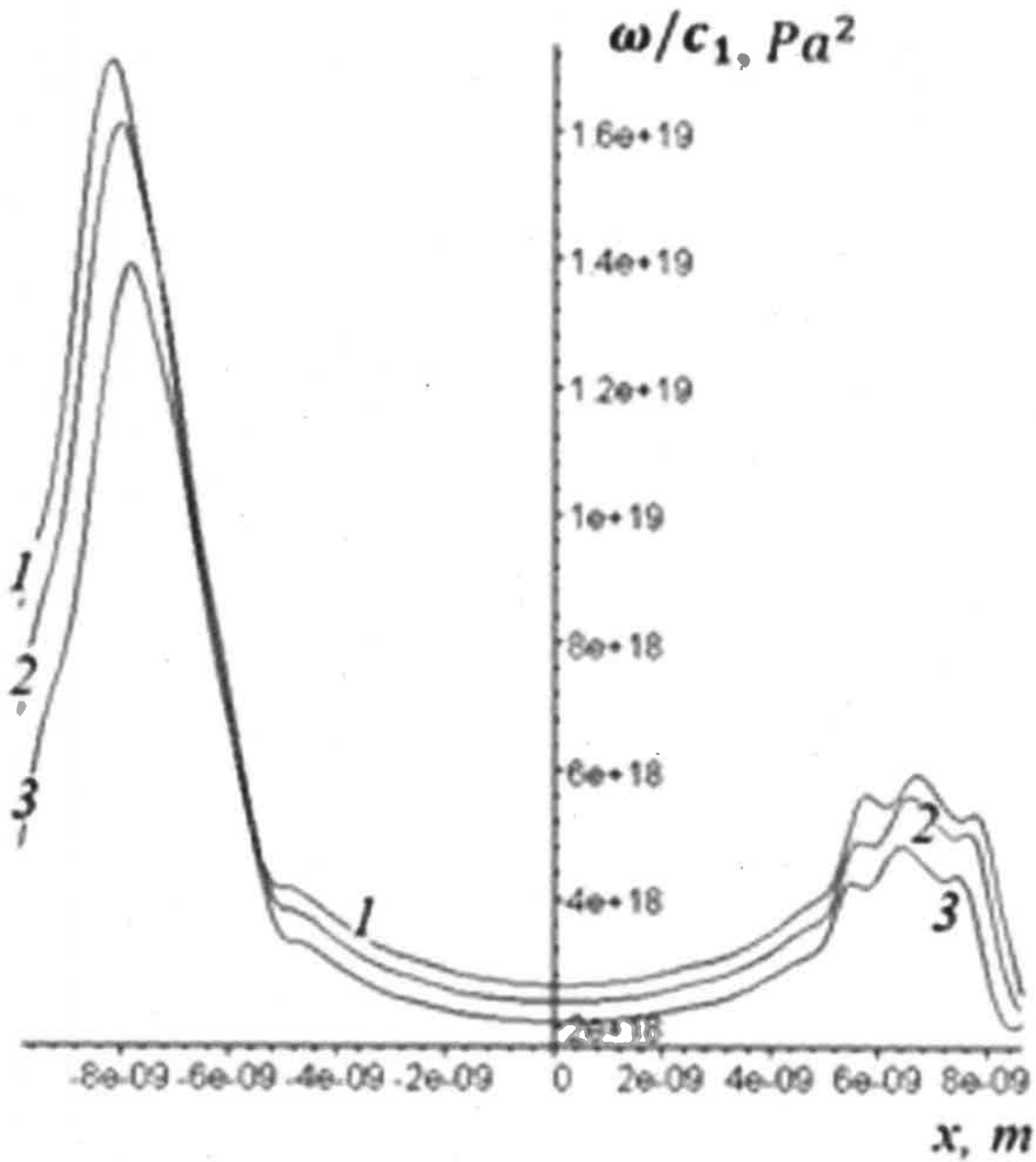
ω/c1, Pa2
1.6e+19
1.4e+19
1.2e+19
1e+19
8e+18
6e+18
4e+18
1
2
3
-8e-09
-6e-09
-4e-09
-2e-09
0
2e-09
4e-09
6e-09
8e-09
x, m